

MeV-scale reheating temperature and thermalization of oscillating neutrinos by radiative and hadronic decays of massive particles

Takuya Hasegawa,^{1,2} Nagisa Hiroshima,^{1,3,4} Kazunori Kohri,^{1,2,5}
Rasmus S. L. Hansen,^{6,7} Thomas Tram,^{7,8} and Steen Hannestad⁷

¹*Theory Center, IPNS, KEK, Tsukuba 305-0801, Japan*

²*The Graduate University of Advanced Studies (Sokendai), Tsukuba 305-0801, Japan*

³*RIKEN Interdisciplinary Theoretical and Mathematical
Sciences (iTHEMS), Wako, Saitama 351-0198, Japan*

⁴*Institute for Cosmic Ray Research, University of Tokyo, Kashiwa, Chiba 277-8582, Japan*

⁵*Kavli IPMU (WPI), UTIAS, The University of Tokyo, Kashiwa, Chiba 277-8583, Japan*

⁶*Max-Planck-Institut für Kernphysik, Saupfercheckweg 1, 69117 Heidelberg, Germany*

⁷*Department of Physics and Astronomy, University of Aarhus,
Ny Munkegade 120, DK8000 Aarhus C, Denmark*

⁸*Aarhus Institute of Advanced Studies (AIAS),
Aarhus University, DK8000 Aarhus C, Denmark*

(Dated: December 10, 2019)

From a theoretical point of view, there is a strong motivation to consider an MeV-scale reheating temperature induced by long-lived massive particles with masses around the weak scale, decaying only through gravitational interaction. In this study, we investigate lower limits on the reheating temperature imposed by big-bang nucleosynthesis assuming both radiative and hadronic decays of such massive particles. For the first time, effects of neutrino self-interactions and oscillations are taken into account in the neutrino thermalization calculations. By requiring consistency between theoretical and observational values of light element abundances, we find that the reheating temperature should conservatively be $T_{\text{RH}} \gtrsim 1.8$ MeV in the case of the 100% radiative decay, and $T_{\text{RH}} \gtrsim 4\text{--}5$ MeV in the case of the 100% hadronic decays for particle masses in the range of 10 GeV to 100 TeV.

I. INTRODUCTION

In the standard big-bang cosmology it is normally assumed that radiation components (photons, electrons/positrons, and neutrinos) were perfectly thermalized, and energy of radiation dominated the total energy density of the Universe well before the beginning of big-bang nucleosynthesis (BBN). In a modern picture of the early Universe, this radiation-dominated epoch is expected to be realized after a decay of a massive particle such as the inflaton, the particle associated with the inflaton field driving inflation, or another massive particle such as the curvaton. If such massive particles abundantly existed in the early Universe, their non-relativistic energy could dominate the total energy, and then an early matter-dominated epoch should have been realized before the radiation-dominated epoch. Therefore, particle production caused by their decays and subsequent entropy production (called reheating) dramatically modify the thermal history of the Universe. The Universe could experience the reheating more than once after inflation depending on the fundamental theory of particle physics. Since many theoretical models have been proposed as a theory beyond the standard model of particle physics, it is required to have some ways to find the true theory of nature. The one of the approaches is to investigate the possible value of “reheating temperature” which is defined by the cosmic temperature when the radiation-dominated epoch just started. This is because the reheating temperature is related to the property of the massive particles, and we can constrain the theories through the observational bound on the reheating temperature.

As for a candidate of inflaton field or curvaton field, a lot of unstable massive scalar fields, *e.g.* moduli, dilaton fields, are predicted in particle physics theories beyond the standard model such as supergravity or superstring theory. They tend to dominate the total energy of the Universe during their oscillation epochs. It is notable that they typically have masses at or above the weak scale and decay only through gravitational interaction. This means that they have long lifetimes of $\mathcal{O}(0.1)$ sec– $\mathcal{O}(10)$ sec, and the reheating temperature after their decay is expected to be $\mathcal{O}(1)$ MeV. Since neutrinos decoupled from the thermal plasma at around the cosmic temperature $T \sim \mathcal{O}(1)$ MeV, they would have suffered imperfect thermalization due to the late-time entropy production caused by their decay. Thus, we have a strong motivation to observationally test this kind of cosmological scenarios with decaying particles which induce the MeV-scale reheating temperature.

The theory of BBN based on the standard big-bang cosmology, *i.e.* standard BBN, successfully explains observational light element abundances (see *e.g.* Ref. [1] and references therein), and the

theory say that the light elements are synthesized at around $T \sim \mathcal{O}(0.01)$ MeV– $\mathcal{O}(0.1)$ MeV. As we shall see in Sec. IV, BBN is highly sensitive to the neutrino abundances. Therefore, we can examine the MeV-scale reheating scenarios by using BBN as a probe.

In Ref. [2], lower bounds on reheating temperature have been studied in terms of BBN for the first time. They have shown that an incomplete thermalization of neutrinos gives the most significant effect on BBN assuming that the 100% of the long-lived massive particles decay into electromagnetic radiations such as photons or charged leptons. Because of a competition between decreases and increases of the produced amount of ${}^4\text{He}$ by the imperfect thermalization of the neutrinos, we can constrain the reheating temperature. As a result, they have obtained a conservative lower bound on the reheating temperature $T_{\text{RH}} > 0.5$ MeV– 0.7 MeV (95% C.L.).

Afterwards, in Ref. [3], they discussed hadronic decays of massive particles, *i.e.* direct decays into quarks and/or gluons which immediately fragment into hadrons such as pions, kaons, or nucleons. The thermalization of radiations proceed in exactly the same way as in the case where the 100% of the massive particles decay into electromagnetic radiations. This is because almost all of the kinetic energy of hadrons are transferred into radiation through Coulomb scattering with background electrons/positrons or inverse-Compton like scattering with background photons, and a neutral pion π^0 immediately decays into two photons. In the case of the hadronic decay, interconverting reactions between ambient protons and neutrons induced by emitted hadrons are extraordinarily important because they increase the neutron to proton ratio which is a key parameter of resultant abundances of light elements. As a result, they obtained a lower bound $T_{\text{RH}} > 2.5$ – 4 MeV (95% C.L.) depending on the mass of the long-lived massive particles and their branching ratio into hadrons.

Subsequently, two- and three-flavor neutrino oscillations were respectively considered in the thermalization process of neutrinos in Refs. [4] and [5] where they obtained a lower bound $T_{\text{RH}} > 2$ MeV (95% C.L.) and $T_{\text{RH}} > 4.1$ MeV (95% C.L.) assuming radiative decay of the massive particles.

Some other cosmological probes other than BBN are also sensitive to neutrino abundances. Here we briefly refer to the recent papers which focused on this topic. In Ref. [3], they discussed possible effects of an incomplete thermalization of neutrinos on a temperature anisotropy and polarization of Cosmic Microwave Background (CMB) and a galaxy power spectrum of Large Scale Structure (LSS). Ref. [6] obtained a combined constraint $T_{\text{RH}} > 4$ MeV (95% C.L.) by considering BBN, CMB (WMAP) and LSS (2dF Galaxy Redshift Survey).

After that, authors in Ref. [7] have updated the CMB and LSS data by using WMAP three-

year data and SDSS luminous red galaxies data, and they obtained $T_{\text{RH}} > 2$ MeV (95% C.L.). Similar analysis have been done in Ref. [8] by using WMAP five-year data and SDSS luminous red galaxies data where they obtained $T_{\text{RH}} > 2$ MeV (95% C.L.) from CMB only and $T_{\text{RH}} > 3.2$ MeV (95% C.L.) from CMB by including external priors from SDSS red luminous galaxy survey and the constraint from the comoving age. In addition, authors in Ref. [5] have reported a new constraint $T_{\text{RH}} > 4.3$ MeV (95% C.L.) from CMB by using Planck 2015 data.

In this paper, we extend the study of Ref. [3] by considering neutrino oscillation and neutrino self-interaction in the calculation of the neutrino thermalization. We assume both radiative and hadronic decays of the massive particles and give an updated bound on the reheating temperature set by BBN. This is the first study that considers effects of neutrino self-interactions on the neutrino thermalization to constrain the reheating temperature.

The structure of this paper is as follows. In Sec. II, we introduce the formalism of the neutrino thermalization assuming the MeV-scale reheating temperature. In Sec. III, we show the results of neutrino thermalization in the reheating, and describe how neutrino oscillation and neutrino self-interaction affect the thermalization process. The results of BBN are shown in Sec. IV where we discuss effects of both radiative and hadronic decays on light element abundances. Finally, we draw our conclusion in Sec. V.

II. REHEATING AND NEUTRINO THERMALIZATION

In this section, we describe the neutrino thermalization in the low-reheating-temperature Universe and introduce the key equations.

As described in the previous section, there are some candidate particles in theories going beyond the Standard Model of particle physics which are weakly interacting and decay at around BBN. Here, we call the long-lived massive particles just “massive particles” and label them X . We assume the energy density of the massive particles dominates those of other particles at an initial time and the Universe is completely matter-dominated before the massive particles start to decay. In this setting, the entropy production caused by the decay of X induces particle production via electromagnetic, weak, and strong interactions. As a result, photons and charged leptons are rapidly thermalized in the reheating via electromagnetic interactions, whereas the weakly interacting neutrinos are slowly created in the thermal bath of photons and charged leptons.¹ Since neutrinos decouple from the thermal bath at around a temperature of $\mathcal{O}(1)$ MeV, neutrinos should not be fully thermalized if $T_{\text{RH}} \sim \mathcal{O}(1)$ MeV. A degree of thermalization of neutrinos affects the light element abundances [2]. For this reason, it is especially important to accurately calculate the thermalization of neutrinos in the reheating for $T_{\text{RH}} \sim \mathcal{O}(1)$ MeV. Therefore, next we look into the dynamics of neutrino thermalization in the thermal plasma.

In the Universe with a temperature of $\mathcal{O}(1)$ MeV, electrons and positrons are the only charged leptons which are abundant in the system since the abundances of muons and tau leptons are strongly suppressed by Boltzmann factors. Therefore, neutrinos are mainly produced in the annihilation process of electrons and positrons, $e^- + e^+ \rightarrow \nu_\alpha + \bar{\nu}_\alpha$ where $\alpha = e, \mu, \tau$. Since electron neutrino (ν_e) is not only produced by the neutral-current weak interaction but also by the charged-current one, it tends to be produced more than μ neutrinos (ν_μ) and τ neutrinos (ν_τ) when all neutrinos are not fully thermalized. Consequently, neutrino oscillations play a role in equilibrating neutrino abundances in this case, and we have to simultaneously consider the neutrino production by collisions and flavor oscillations.

Our treatment of neutrino oscillation is consistent with that of Ref. [4]. That is, we adopt the effective two-flavor mixing scheme which is a good description to approximately include full three-flavor mixings when the collision rates of ν_μ and ν_τ are identical, and one mixing angle is

¹ In the case where the massive particles decay into quarks and/or gluons, they fragment into mesons and baryons after the hadronization, and almost all the kinetic energy of hadrons are transferred into radiation due to the reason mentioned before. Therefore, contributions of secondary neutrinos produced by the decay of hadrons can be neglected. However, there is also another possibility that the massive particles directly decays into neutrinos, *e.g.* $X \rightarrow \nu_\alpha + \bar{\nu}_\alpha$ where $\alpha = e, \mu, \tau$ [6]. In this case, electromagnetic plasma is produced only from neutrinos via weak interaction, which gives totally different results of the neutrino thermalization and BBN. We do not consider the possibility in this paper.

predominantly important compared to others (see *e.g.* Ref. [9] for more details on the effective two-flavor mixing scheme). The former condition is well satisfied because of the absence of muons and tau leptons in the system with a temperature of $\mathcal{O}(1)$ MeV. On the other hand, the latter condition is only approximately satisfied since the reactor neutrino mixing θ_{13} is known to be non-negligible compared to other mixings, namely the solar neutrino mixing θ_{12} and the atmospheric neutrino mixing θ_{23} [10]. In later sections, however, we show that the effect of θ_{13} on BBN is very small compared to that of θ_{12} or neutrino self-interaction irrespective of the mass ordering of neutrinos. Therefore, the effective two-flavor mixing scheme (with the solar neutrino mixing) gives a good description of the full three-flavor mixings at least for the current purpose. In this scheme, we label the degenerate state of ν_μ and ν_τ as x neutrinos (ν_x) and consider the flavor mixing between ν_e and ν_x . Also, we label the other neutrino species which does not mix with other flavors as spectator neutrino (ν_{sp}) in this two-flavor treatment.

In general, neutrino states can be described by a one-particle irreducible density matrix $\varrho_{\mathbf{p}} \equiv \varrho(p, t)$ where $p \equiv |\mathbf{p}|$ is the absolute momentum.² Since we focus on the effective two-flavor mixing, the density matrix is expressed in terms of a 2×2 Hermitian matrix, and we label each element of the density matrix as

$$\varrho_{\mathbf{p}} = \begin{pmatrix} \rho_{ee} & \rho_{ex} \\ \rho_{ex}^* & \rho_{xx} \end{pmatrix}. \quad (2.1)$$

The diagonal part of the matrix corresponds to the distribution function of mixed neutrinos (*i.e.* ν_e and ν_x), that is, $\rho_{ee} = f_{\nu_e}$ and $\rho_{xx} = f_{\nu_x}$, while the off-diagonal elements represent the quantum coherence among neutrinos with different flavors. In the current study, the chemical potentials of neutrinos are set to be zero. Under this assumption, the density matrix of neutrinos is equal to that of anti-neutrinos, *i.e.* $\varrho_{\mathbf{p}} = \bar{\varrho}_{\mathbf{p}}$, and they have the same abundance. Therefore, it is not necessary to follow the time evolution of anti-neutrinos separately from that of the corresponding neutrinos.

We can obtain the time evolution of the neutrino density matrix by solving the momentum-dependent Quantum Kinetic Equation [11, 12] which is formally written as

$$\frac{d\varrho_{\mathbf{p}}}{dt} = \frac{\partial\varrho_{\mathbf{p}}}{\partial t} - H p \frac{\partial\varrho_{\mathbf{p}}}{\partial p} = -i[\mathcal{H}_{\mathbf{p}}, \varrho_{\mathbf{p}}] + C(\varrho_{\mathbf{p}}). \quad (2.2)$$

In the above equation, the term including the Hubble parameter H corresponds to the effect of the

² Since we focus on the Universe with a temperature of $\mathcal{O}(1)$ MeV, we can neglect tiny neutrino masses which are known to be sub-eV scale [1]. In this case, energy of neutrinos E is equal to its absolute momentum, *i.e.* $E = p$.

expansion of the Universe, and $C(\varrho_{\mathbf{p}})$ is the collision term of neutrinos expressed as

$$C(\varrho_{\mathbf{p}}) = \begin{pmatrix} R_{\nu_e} & -D\rho_{ex} \\ -D\rho_{ex}^* & R_{\nu_x} \end{pmatrix}, \quad (2.3)$$

where R_{ν_e} and R_{ν_x} are the production rates of ν_e and ν_x , respectively. Also, D is the collisional-damping rate which breaks the flavor coherence among different flavors of neutrinos. In this paper, we adopt a simplified treatment of the damping effects discussed in Ref. [5] and neglect the additional contributions such as ‘‘damping-like terms’’ which appear in Ref. [11]. In the current study, we consider the collisional processes $a(k) + b(p) \rightarrow c(k') + d(p')$ shown in Table. I including those of neutrino self-interaction. In this case, the expressions of the repopulation and the damping terms are [13],

$$\begin{aligned} R_{\nu_\alpha}(k) = & 2\pi \int d\Pi_{k'} d\Pi_{p'} d\Pi_p \delta_E(kp|k'p') \\ & \times \sum_i \mathcal{V}^2[\nu_\alpha(k), \bar{\nu}_\alpha(p)|i(k'), \bar{i}(p')] [f_i(E_{k'}) f_{\bar{i}}(E_{p'}) (1 - f_{\nu_\alpha}(k)) (1 - f_{\bar{\nu}_\alpha}(p)) \\ & \quad - f_{\nu_\alpha}(k) f_{\bar{\nu}_\alpha}(p) (1 - f_i(E_{k'})) (1 - f_{\bar{i}}(E_{p'}))] \\ & + \sum_j \mathcal{V}^2[\nu_\alpha(k), j(p)|\nu_\alpha(k'), j(p')] [f_{\nu_\alpha}(k') f_j(E_{p'}) (1 - f_{\nu_\alpha}(k)) (1 - f_j(E_p)) \\ & \quad - f_{\nu_\alpha}(k) f_j(E_p) (1 - f_{\nu_\alpha}(k')) (1 - f_j(E_{p'}))] , \end{aligned} \quad (2.4)$$

$$\begin{aligned} D(k) = & \pi \sum_\alpha \int d\Pi_{k'} d\Pi_{p'} d\Pi_p \delta_E(kp|k'p') \\ & \times \sum_i \mathcal{V}^2[\nu_\alpha(k), \bar{\nu}_\alpha(p)|i(k'), \bar{i}(p')] [f_i(E_{k'}) f_{\bar{i}}(E_{p'}) (1 - f_{\bar{\nu}_\alpha}(p)) \\ & \quad + f_{\bar{\nu}_\alpha}(p) (1 - f_{\bar{i}}(E_{p'})) (1 - f_i(E_{k'}))] \\ & + \sum_j \mathcal{V}^2[\nu_\alpha(k), j(p)|\nu_\alpha(k'), j(p')] [f_{\nu_\alpha}(k') f_j(E_{p'}) (1 - f_j(E_p)) \\ & \quad + f_j(E_p) (1 - f_j(E_{p'})) (1 - f_{\nu_\alpha}(k'))] , \end{aligned} \quad (2.5)$$

where $\alpha = e, x$, and k, p, k' and p' are absolute momenta of the particle a, b, c and d , respectively. Also, $d\Pi_p \equiv \frac{d^3\mathbf{p}}{(2\pi)^3}$, and $\delta_E(kp|k'p') \equiv \delta^{(1)}(E_k + E_p - E_{k'} - E_{p'})$ is the 1D Dirac delta function corresponding to energy conservation for each process. The summation index i runs over electrons and all flavors of neutrinos other than ν_α (*i.e.* ν_β where $\beta \neq \alpha$), while j runs in addition over positrons, ν_α , and all flavors of anti-neutrinos. The expression of \mathcal{V}^2 is written as

$$\mathcal{V}^2[a(p), b(k)|c(p'), d(k')] = (2\pi)^3 \delta^{(3)}(k+p, k'+p') N_a^2 N_b^2 N_c^2 N_d^2 S |M|^2(a(p), b(k)|c(p'), d(k')), \quad (2.6)$$

Process ($\alpha \neq \beta$)	$S M ^2$
I. $e^- + e^+ \rightarrow \nu_\alpha + \bar{\nu}_\alpha$	$2^5 G_F^2 [(2 \sin^2 \theta_W \pm 1)^2 (k \cdot p')(p \cdot k') + 4 \sin^4 \theta_W (k \cdot k')(p \cdot p') + 2 m_e^2 \sin^2 \theta_W (2 \sin^2 \theta_W \pm 1)(k \cdot p)]$
II. $\nu_\alpha + e^+ \rightarrow \nu_\alpha + e^+$	$2^5 G_F^2 [(2 \sin^2 \theta_W \pm 1)^2 (k \cdot k')(p \cdot p') + 4 \sin^4 \theta_W (k \cdot p)(k' \cdot p') - 2 m_e^2 \sin^2 \theta_W (2 \sin^2 \theta_W \pm 1)(k \cdot p')]$
III. $\nu_\alpha + e^- \rightarrow \nu_\alpha + e^-$	$2^5 G_F^2 [(2 \sin^2 \theta_W \pm 1)^2 (k \cdot p)(k' \cdot p') + 4 \sin^4 \theta_W (k \cdot k')(p \cdot p') - 2 m_e^2 \sin^2 \theta_W (2 \sin^2 \theta_W \pm 1)(k \cdot p')]$
IV. $\nu_\alpha + \nu_\alpha \rightarrow \nu_\alpha + \nu_\alpha$	$2^6 G_F^2 (k \cdot p)(k' \cdot p')$
V. $\nu_\alpha + \nu_\beta \rightarrow \nu_\alpha + \nu_\beta$	$2^5 G_F^2 (k \cdot p)(k' \cdot p')$
VI. $\nu_\alpha + \bar{\nu}_\alpha \rightarrow \nu_\alpha + \bar{\nu}_\alpha$	$2^7 G_F^2 (k \cdot p')(p \cdot k')$
VII. $\nu_\alpha + \bar{\nu}_\beta \rightarrow \nu_\alpha + \bar{\nu}_\beta$	$2^5 G_F^2 (k \cdot p')(p \cdot k')$
VIII. $\nu_\alpha + \bar{\nu}_\alpha \rightarrow \nu_\beta + \bar{\nu}_\beta$	$2^5 G_F^2 (k \cdot p')(p \cdot k')$

Table. I. Collision process $a(p) + b(k) \rightarrow c(p') + d(k')$ which contributes to the thermalization of neutrinos of each flavor ν_α, ν_β ($\alpha, \beta = e, \mu, \tau$ where $\alpha \neq \beta$). The process I is the production process of neutrinos due to electron annihilation, the processes II–III are the scattering processes between neutrinos and electrons, and the processes IV–VIII are the self-interaction processes among neutrinos. Here, θ_W is the Weinberg angle, G_F is the Fermi-coupling constant, S is the symmetry factor, and $|M|^2$ is the squared scattering matrix element. The positive sign in the expression is for ν_e and the minus sign for ν_μ or ν_τ (*i.e.* for ν_x and ν_{sp}). The expressions of the process I, II, IV and V are also applied to the corresponding anti-neutrinos.

where $S|M|^2(a(p), b(k)|c(p'), d(k'))$ is the squared scattering matrix element for the processes in Table. I summed over initial and final spins, and symmetrized over identical particles in the initial and the final state. Also, $N_i \equiv \sqrt{1/2E_i}$ where E_i is the energy of particle i ($i = a, b, c, d$) and $\delta^{(3)}(k + p, k' + p') \equiv \delta^{(3)}(\mathbf{k} + \mathbf{p} - \mathbf{k}' - \mathbf{p}')$ is the 3D Dirac delta function corresponding to the momentum conservation. As for the processes in Table. I, we analytically reduce the dimension of momentum integrals in the above expressions from nine to two and calculate the full collision terms without any simplifying assumptions in the same way as in Ref. [13].

In the expression of Eq. (2.2), \mathcal{H}_p is neutrino Hamiltonian which is expressed as

$$\mathcal{H}_p = \mathcal{H}_{p, \text{vac}} + \mathcal{H}_{p, \text{mat}} = \frac{M^2}{2p} - \frac{8\sqrt{2}G_F p}{3} \left[\frac{E_l}{m_W^2} + \frac{E_\nu}{m_Z^2} \right] + \sqrt{2}G_F \int d\Pi_{p'} (\varrho_{p'} - \bar{\varrho}_{p'}^*), \quad (2.7)$$

where G_F is the Fermi-coupling constant. Also, m_W and m_Z are the masses of W and Z bosons, respectively. In the above expression, the first term, $\mathcal{H}_{p, \text{vac}}$, is the contribution which induces the vacuum oscillation where M is the mass matrix in flavor basis. The mass matrix M is related to the one in mass basis \mathcal{M} as $M^2 = U\mathcal{M}^2U^\dagger$ where U is the PMNS matrix. In the effective two-flavor

mixing scheme,

$$\mathcal{M}^2 = \begin{pmatrix} m_1^2 & 0 \\ 0 & m_2^2 \end{pmatrix}, \quad U = \begin{pmatrix} \cos \theta & \sin \theta \\ -\sin \theta & \cos \theta \end{pmatrix}, \quad (2.8)$$

where $\delta m^2 \equiv m_2^2 - m_1^2$ is the squared-mass difference and θ is the mixing angle in vacuum between ν_e and ν_x . Also, the second term in the Hamiltonian, $\mathcal{H}_{\mathbf{p}, \text{mat}}$, corresponds to the matter potentials which arise from coherent scatterings between neutrinos and charged-leptons. In the term, \mathbf{E}_l corresponds to the total energy density of charged leptons, while \mathbf{E}_ν to that of neutrinos:

$$\mathbf{E}_l = \begin{pmatrix} \rho_e & 0 \\ 0 & 0 \end{pmatrix}, \quad \mathbf{E}_\nu = \int d\Pi_{p'} p' (\varrho_{\mathbf{p}'} + \bar{\varrho}_{\mathbf{p}'}^*) = \begin{pmatrix} \rho_{\nu_e} & \rho_{\nu_{ex}} \\ \rho_{\nu_{ex}}^* & \rho_{\nu_x} \end{pmatrix}, \quad (2.9)$$

where $\rho_e = \rho_{e^-} + \rho_{e^+}$ is the total energy density of electrons and positrons, while ρ_{ν_e} and ρ_{ν_x} are those of ν_e and ν_x , respectively. Also, we have defined $\rho_{\nu_{ex}} \equiv \int d\Pi_{p'} p' (\rho_{ex} + \bar{\rho}_{ex}^*)$ and $\rho_{\nu_{ex}}^* \equiv \int d\Pi_{p'} p' (\rho_{ex}^* + \bar{\rho}_{ex})$. In the expression of \mathbf{E}_l , we have neglected the existence of muons or tau leptons due to their large masses.³ The asymmetric part of $\mathcal{H}_{\mathbf{p}, \text{mat}}$ is often assumed to vanish when $\rho = \bar{\rho}$ for neutrinos and the number density of electrons and positrons are identical. For the diagonal part of the Hamiltonian this is true, however the off-diagonal part gets a contribution from the neutrinos as shown in Eq. (2.7) since $\varrho_{\mathbf{p}}^* \neq \varrho_{\mathbf{p}}$.

As for the oscillation parameters, we use the best fit values of the mass-squared differences and mixing angles reported in Ref. [10]:⁴

$$\delta m_{12}^2 = 7.55 \times 10^{-5} \text{ eV}^2, \quad \sin^2 \theta_{12} = 3.20 \times 10^{-1}, \quad (2.10)$$

$$\delta m_{13}^2 = 2.50 \times 10^{-3} \text{ eV}^2, \quad \sin^2 \theta_{13} = 2.160 \times 10^{-2} \text{ (NO)}, \quad (2.11)$$

$$\delta m_{13}^2 = -2.42 \times 10^{-3} \text{ eV}^2, \quad \sin^2 \theta_{13} = 2.220 \times 10^{-2} \text{ (IO)}, \quad (2.12)$$

where ‘‘NO’’ (‘‘IO’’) means normal (inverted) mass ordering of neutrinos, respectively. For the numerical calculation, we rewrite the 2×2 density matrix with polarization vectors (P_0, \mathbf{P}):

$$\varrho_{\mathbf{p}} = \begin{pmatrix} \rho_{ee} & \rho_{ex} \\ \rho_{ex}^* & \rho_{xx} \end{pmatrix} = \frac{1}{2} [P_0(p) \sigma_0 + \mathbf{P}(p) \cdot \boldsymbol{\sigma}], \quad (2.13)$$

where $\sigma_0 = \mathbf{1}$ is the identity matrix and $\boldsymbol{\sigma} = (\sigma_x, \sigma_y, \sigma_z)$ are the Pauli matrices. With $\mathbf{P} = (P_x, P_y, P_z)$, distribution functions of mixed neutrinos can be written as

$$f_{\nu_e} = \frac{1}{2}(P_0 + P_z), \quad f_{\nu_x} = \frac{1}{2}(P_0 - P_z). \quad (2.14)$$

³ In the effective two-flavor mixing scheme, we need to treat both ν_μ and ν_τ in the same way. Therefore, we do not consider background muons or tau leptons whose contribution is very small compared to that of electrons.

⁴ The atmospheric neutrino mixing ($\theta_{23}, \delta m_{23}^2$) is irrelevant to the oscillation between ν_e and ν_x in the effective two-flavor mixing scheme. Therefore, we do not use the value in this paper.

In addition, we can rewrite the expression of Eq. (2.2) as follows:

$$\dot{\mathbf{P}} = \vec{\mathcal{H}} \times \mathbf{P} - D(P_x \mathbf{x} + P_y \mathbf{y}) + (R_{\nu_e} - R_{\nu_x}) \mathbf{z}, \quad (2.15)$$

$$\dot{P}_0 = R_{\nu_e} + R_{\nu_x}, \quad (2.16)$$

which leads to

$$\dot{P}_{\nu_e} = \mathcal{H}_x P_y - \mathcal{H}_y P_x + 2 R_{\nu_e}, \quad (2.17)$$

$$\dot{P}_{\nu_x} = \mathcal{H}_y P_x - \mathcal{H}_x P_y + 2 R_{\nu_x}, \quad (2.18)$$

$$\dot{P}_x = \frac{1}{2} \mathcal{H}_y (P_{\nu_e} - P_{\nu_x}) - \mathcal{H}_z P_y - D P_x, \quad (2.19)$$

$$\dot{P}_y = \mathcal{H}_z P_x - \frac{1}{2} \mathcal{H}_x (P_{\nu_e} - P_{\nu_x}) - D P_y, \quad (2.20)$$

where \mathbf{x}, \mathbf{y} and \mathbf{z} are unit vectors, and we defined $P_{\nu_e} \equiv P_0 + P_z$ and $P_{\nu_x} \equiv P_0 - P_z$. Each component of the neutrino potential $\vec{\mathcal{H}}$, *i.e.* $\mathcal{H}_i = \text{Tr}(\mathcal{H}_{\mathbf{p}} \sigma_i)$ where $i = x, y, z$, is written as

$$\mathcal{H}_x = \frac{\delta m^2}{2p} \sin 2\theta - \frac{16\sqrt{2} G_F p}{3 m_Z^2} \int d\Pi_{p'} p' P_x, \quad (2.21)$$

$$\mathcal{H}_y = 2\sqrt{2} G_F \int d\Pi_{p'} P_y, \quad (2.22)$$

$$\mathcal{H}_z = -\frac{\delta m^2}{2p} \cos 2\theta + \mathcal{H}_{\text{mat}}. \quad (2.23)$$

The second term in \mathcal{H}_z is the matter contribution which is explicitly written as

$$\mathcal{H}_{\text{mat}} = -\frac{8\sqrt{2}}{3} G_F p \left[\frac{\rho_e}{m_W^2} + \frac{\rho_{\nu_e} - \rho_{\nu_x}}{m_Z^2} \right], \quad (2.24)$$

$$= -\frac{4\sqrt{2}}{3\pi^2} G_F p \left[\frac{g_e}{m_W^2} \int_0^\infty dp' p'^2 \frac{E_e}{\exp(E_e/T_\gamma) + 1} + \frac{g_\nu}{m_Z^2} \int_0^\infty dp' p'^3 (f_{\nu_e} - f_{\nu_x}) \right], \quad (2.25)$$

where T_γ is the photon temperature, and $E_e = \sqrt{p^2 + m_e^2}$ is the energy of electrons. Also, $g_e = 4$ is statistical degree of freedom of electrons and $g_\nu = 2$ is that of neutrinos of each flavor.

With the matter potential \mathcal{H}_{mat} , the mass-squared difference and the mixing angle in vacuum are modified in medium by MSW effect as follows [14, 15]:

$$\frac{\delta m_M^2}{2p} = \sqrt{\left(\frac{\delta m^2}{2p}\right)^2 \sin^2 2\theta + \left(-\frac{\delta m^2}{2p} \cos 2\theta + \mathcal{H}_{\text{mat}}\right)^2}, \quad (2.26)$$

$$\sin^2 2\theta_M = \frac{\left(\frac{\delta m^2}{2p}\right)^2 \sin^2 2\theta}{\left(\frac{\delta m^2}{2p}\right)^2 \sin^2 2\theta + \left(-\frac{\delta m^2}{2p} \cos 2\theta + \mathcal{H}_{\text{mat}}\right)^2}, \quad (2.27)$$

where δm_M^2 and θ_M are the in-medium mass-squared difference and the mixing angle, respectively. We note here that in Eqs. (2.26)–(2.27) we simplify the expressions by neglecting the small contributions of the off-diagonal part of the matter potential $\mathcal{H}_{\mathbf{p}, \text{mat}}$ in Eq. (2.7) (see Ref. [9] for the exact expressions of the MSW effect). As can be seen from Eqs. (2.26) and (2.27), the matter potential $|\mathcal{H}_{\text{mat}}| \propto T_\gamma^5$ dominates the vacuum one $|\mathcal{H}_{\text{vac}}| \equiv |-\frac{\delta m^2}{2p} \cos 2\theta| \propto T_\gamma^{-1}$, *i.e.* $|\mathcal{H}_{\text{mat}}| \gg |\mathcal{H}_{\text{vac}}|$, at high temperature such as $T_\gamma > \mathcal{O}(10)$ MeV and $\theta_M \sim 0$ holds for most energy modes.⁵ On the other hand, the opposite hierarchy, *i.e.* $|\mathcal{H}_{\text{vac}}| \gg |\mathcal{H}_{\text{mat}}|$, holds at low temperature and the mixing parameters take the same values as those in vacuum: $\theta_M \sim \theta$, $\delta m_M^2 \sim \delta m^2$. For neutrinos with momentum $p = \langle p \rangle \sim 3.15 T_\gamma$ where $\langle \cdot \rangle$ means a thermal average, the level crossing between these potentials, *i.e.* $|\mathcal{H}_{\text{mat}}| \sim |\mathcal{H}_{\text{vac}}|$, occurs at the temperature T_c

$$T_c \sim G_{\text{F}}^{-1/3} (\delta m^2 \cos 2\theta)^{1/6} \sim \begin{cases} 3 \text{ MeV} \left(\frac{\delta m_{12}^2}{2.5 \times 10^{-3} \text{ eV}^2} \right)^{1/6} \\ 5 \text{ MeV} \left(\frac{\delta m_{13}^2}{7.5 \times 10^{-5} \text{ eV}^2} \right)^{1/6} \end{cases}, \quad (2.28)$$

where, in the above evaluation, we have replaced p with $\langle p \rangle \sim 3.15 T_\gamma$ and approximated $(\cos 2\theta)^{1/6} \sim 1$ which is well satisfied for θ_{12} and θ_{13} . Therefore, neutrino oscillation becomes effective at around a temperature of $\mathcal{O}(1)$ MeV for the solar neutrino mixing ($\theta_{12}, \delta m_{12}$) and the reactor neutrino mixing ($\theta_{13}, \delta m_{13}$), which is the reason for taking its effect on the neutrino thermalization into account.

On the other hand, since ν_{sp} decouple from flavor mixings of neutrinos, the time evolution of this neutrino species is just given by the classical Boltzmann equation:

$$\frac{df_{\nu_{\text{sp}}}}{dt} = \frac{\partial f_{\nu_{\text{sp}}}}{\partial t} - H p \frac{\partial f_{\nu_{\text{sp}}}}{\partial p} = C(f_{\nu_{\text{sp}}}), \quad (2.29)$$

where $f_{\nu_{\text{sp}}}$ is the distribution function of ν_{sp} , and $C(f_{\nu_{\text{sp}}})$ is the collision term whose expression is equal to that of ν_x , *i.e.* $C(f_{\nu_{\text{sp}}}) = R_{\nu_x}$ (see Eq. (2.4)).

In order to calculate the thermalization process of neutrinos in the expanding Universe, we also need to compute the energy conservation equation:

$$\frac{d\rho}{dt} = -3H(\rho + P), \quad (2.30)$$

which can be expressed as the time evolution of the photon temperature T_γ :

$$\frac{dT_\gamma}{dt} = -\frac{-\Gamma_X \rho_X + 4H(\rho_\gamma + \rho_\nu) + 3H(\rho_e + P_e) + \frac{d\rho_\nu}{dt}}{\frac{\partial \rho_\gamma}{\partial T_\gamma}|_{a(t)} + \frac{\partial \rho_e}{\partial T_\gamma}|_{a(t)}}, \quad (2.31)$$

⁵ We assume here that the neutrinos are thermalized with photons and have a temperature T_γ for simplicity.

where $a(t)$ is the scale factor at the cosmic time t , Γ_X is the decay rate of the massive particles, whereas ρ and P are the total energy density and the total pressure, respectively:

$$\begin{aligned} \rho &= \rho_\gamma + \rho_e + \rho_\nu + \rho_X, \\ &= \frac{\pi^2}{15} T_\gamma^4 + \frac{g_e}{2\pi^2} \int_0^\infty dp' p'^2 \frac{E_e}{\exp(E_e/T_\gamma) + 1} \\ &\quad + \frac{g_\nu}{2\pi^2} \int_0^\infty dp' p'^3 (f_{\nu_e} + f_{\nu_x} + f_{\nu_{\text{sp}}}) + \rho_X, \end{aligned} \quad (2.32)$$

$$\begin{aligned} P &= P_\gamma + P_e + P_\nu, \\ &= \frac{\pi^2}{45} T_\gamma^4 + \frac{g_e}{6\pi^2} \int_0^\infty dp' \frac{p'^4}{E_e} \frac{1}{\exp(E_e/T_\gamma) + 1} \\ &\quad + \frac{g_\nu}{6\pi^2} \int_0^\infty dp' p'^3 (f_{\nu_e} + f_{\nu_x} + f_{\nu_{\text{sp}}}). \end{aligned} \quad (2.33)$$

Here, $\rho_\gamma(P_\gamma)$, $\rho_e(P_e)$, $\rho_\nu(P_\nu)$ and ρ_X mean the energy density (pressure) of photons, electrons, neutrinos and the massive particles, respectively. The total energy density and the total pressure of neutrinos are a sum of three contributions: $\rho_\nu = \rho_{\nu_e} + \rho_{\nu_x} + \rho_{\nu_{\text{sp}}}$, $P_\nu = P_{\nu_e} + P_{\nu_x} + P_{\nu_{\text{sp}}}$. In addition, the Hubble parameter H is obtained by solving the Friedmann equation:

$$H \equiv \frac{\dot{a}}{a} = \sqrt{\frac{8\pi G\rho}{3}}. \quad (2.34)$$

In the above expression, we can obtain the time evolution of ρ_X by solving the Boltzmann equation of the massive particles X :

$$\frac{d\rho_X}{dt} = -\Gamma_X \rho_X - 3H\rho_X, \quad (2.35)$$

which can be integrated analytically for non-relativistic particles X :

$$\frac{\rho_X}{s} = \frac{\rho_{X,0}}{s_0} e^{-\Gamma_X t}, \quad (2.36)$$

where $\rho_{X,0}$ and s_0 are respectively the initial energy- and entropy density of X , and $\rho_{X,0}$ is assumed to be much larger than those of other particles, *i.e.* $\rho_{X,0} \gg (\rho_\gamma + \rho_e + \rho_\nu)_{t=0}$. In addition, Γ_X is related to T_{RH} through the Hubble parameter $H = H(T_{\text{RH}})$ as follows:

$$\Gamma_X = 3H. \quad (2.37)$$

Since the energy density of the Universe is dominated by radiation components after most of the massive particles decayed and $T_\gamma \sim T_{\text{RH}}$ is realized, we can approximately write the Hubble parameter as

$$H = \sqrt{\frac{g^* \pi^2}{90} \frac{T_{\text{RH}}^2}{m_{\text{pl}}}}, \quad (2.38)$$

where $m_{\text{pl}} \sim 2.435 \times 10^{18}$ GeV is the reduced Planck mass, and $g^* = 10.75$ is the relativistic degrees of freedom in the Universe with a temperature of $\mathcal{O}(1)$ MeV. Hence, the relation between T_{RH} and the decay rate of X is approximately written as

$$T_{\text{RH}} \sim 0.7 \left(\frac{\Gamma_X}{\text{sec}^{-1}} \right)^{1/2} \text{ MeV} . \quad (2.39)$$

From the above expression, we can see that $T_{\text{RH}} \sim \mathcal{O}(1)$ MeV corresponds to the lifetime of the massive particles $\tau_X = \Gamma_X^{-1} \sim \mathcal{O}(1)$ sec.⁶ In order to obtain the neutrino distribution functions and a degree of the neutrino thermalization in the reheating, we simultaneously solve the Eqs. (2.17), (2.18), (2.19), (2.20), (2.29), (2.31), (2.34) and (2.36) from the initial time $t = 10^{-4}$ sec to the final time $t = 10^7$ sec corresponding to the cosmic time well before and after BBN, respectively. We find that the final results are independent of the choice of the initial time as long as the initial temperature of electromagnetic particles is much higher than T_{RH} . To calculate neutrino thermalization processes, we use a modified version of LASAGNA code [16, 17] which is, in the original version, a solver of ordinary differential equations for calculating sterile neutrino production in the early Universe.

In the next section, we show our numerical results of the neutrino thermalization and BBN in the low-reheating-temperature Universe.

⁶ Since the actual value of g^* depends on the value of T_{RH} , Eq. (2.37) just gives a rough estimate of when the radiation-dominated epoch is realized.

III. NUMERICAL RESULTS: NEUTRINO THERMALIZATION IN THE REHEATING

In this section, we show our numerical results of neutrino thermalization. In order to express the time evolution of the neutrino thermalization, we define the effective number of neutrino species N_{eff} :

$$N_{\text{eff}} = N_{\text{eff},\nu_e} + N_{\text{eff},\nu_x} + N_{\text{eff},\nu_{\text{sp}}} = \sum_{\alpha=e,x,\text{sp}} \rho_{\nu_\alpha} / \rho_{\nu_{\alpha,\text{std}}}, \quad (3.1)$$

where $N_{\text{eff},\nu_\alpha}$ is the contribution for each neutrino species, and $\rho_{\nu_{\alpha,\text{std}}}$ is the energy density of each neutrino species in the standard big-bang cosmology.⁷ The value of N_{eff} is almost equal to the actual number of neutrino species when all neutrinos are fully thermalized.

Figure 1 shows the relation between T_{RH} and N_{eff} for the cases with and without neutrino self-interaction. As shown in Fig. 1, the value of N_{eff} increases as T_{RH} becomes large, and the value is almost equal to 3.046 above $T_{\text{RH}} \gtrsim 10$ MeV which is the canonical value in the standard big-bang cosmology with large T_{RH} [18, 19]. The above threshold value of T_{RH} arises from the fact that weak reaction processes which are responsible for the neutrino thermalization decouple at around a temperature T_{dec} given by $\Gamma_{\text{weak}}/H \sim G_F^2 T_{\text{dec}}^5 / (T_{\text{dec}}^2 / m_{\text{pl}}) \sim 1$, *i.e.* $T_{\text{dec}} \sim (G_F^2 m_{\text{pl}})^{-\frac{1}{3}} \sim \mathcal{O}(1)$ MeV where Γ_{weak} is the thermal reaction rate of weakly-interacting particles. Therefore, if T_{RH} is larger than T_{dec} , neutrinos have enough time to be fully thermalized before decoupling. In addition, it can be seen from Fig. 1 that both neutrino oscillation and neutrino self-interaction increase the value of N_{eff} . This is because the production rate of ν_e is larger than that of ν_x ($R_{\nu_e} > R_{\nu_x}$), and thereby neutrino oscillation increases the total production rate of neutrinos $R_{\nu,\text{tot}} (\equiv R_{\nu_e} + R_{\nu_x})$. To understand this effect more quantitatively, let us assume that all neutrino species are almost thermalized. In this case, we can approximate the production rates of ν_e and ν_x as [20]

$$R_{\nu_e} \sim C_e G_F^2 T_\gamma^5 (f_{\text{eq}} - f_{\nu_e}), \quad (3.2)$$

$$R_{\nu_x} \sim C_x G_F^2 T_\gamma^5 (f_{\text{eq}} - f_{\nu_x}), \quad (3.3)$$

where f_{eq} is the Fermi-Dirac distribution $f_{\text{eq}} = 1/(1 + \exp(p/T_\gamma))$, and f_{ν_e} and f_{ν_x} are distribution functions of ν_e and ν_x , respectively. Also, $C_e \sim 1.27$ is the collision coefficient for ν_e and $C_x \sim 0.92$ is that for ν_x [21]. By denoting the effect of neutrino oscillation at a certain time by $\Delta f \equiv f_\nu|_{\text{withosci}} - f_\nu|_{\text{noosci}} \equiv -\Delta f_{\nu_e} = \Delta f_{\nu_x}$, we can evaluate the effect of neutrino oscillation on the total production rate of neutrinos $\Delta R_{\nu,\text{tot}} \equiv R_{\nu,\text{tot}}|_{\text{withosci}} - R_{\nu,\text{tot}}|_{\text{noosci}} = (R_{\nu_e}|_{\text{withosci}} + R_{\nu_x}|_{\text{withosci}}) -$

⁷ The energy density of ν_e is slightly larger than those of ν_x and ν_{sp} after electron annihilation due to the larger reaction rate of ν_e with electrons. Therefore, we discriminate among $\rho_{\nu_{\alpha,\text{std}}}$ with different flavors.

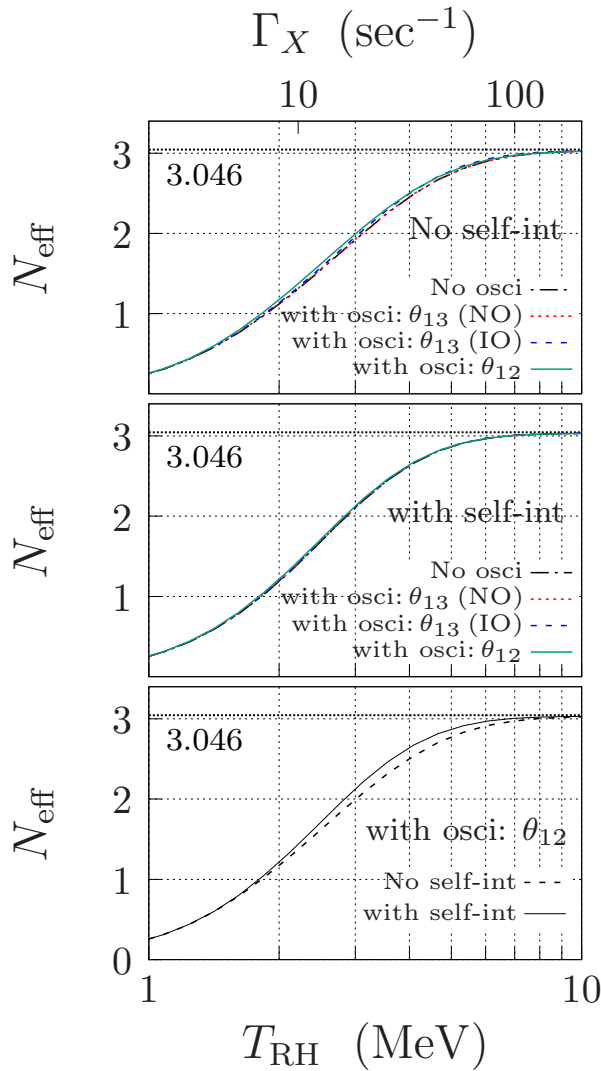


Fig. 1. Relations between T_{RH} and N_{eff} . The top- and middle panels respectively show the effect of neutrino oscillation in the case without and with neutrino self-interaction, while the bottom one shows the effect of neutrino self-interaction in the case with θ_{12} . The canonical value $N_{\text{eff}} = 3.046$ [18] is also plotted with the black dotted horizontal line.

$(R_{\nu_e}|_{\text{no osci}} + R_{\nu_x}|_{\text{no osci}}) = (R_{\nu_e}|_{\text{with osci}} - R_{\nu_e}|_{\text{no osci}}) + (R_{\nu_x}|_{\text{with osci}} - R_{\nu_x}|_{\text{no osci}}) \equiv \Delta R_{\nu_e} + \Delta R_{\nu_x}$ as follows:

$$\begin{aligned}
 \Delta R_{\nu, \text{tot}} &= \Delta R_{\nu_e} + \Delta R_{\nu_x}, \\
 &\sim G_F^2 T_\gamma^5 (-C_e \Delta f_{\nu_e} - C_x \Delta f_{\nu_x}), \\
 &= G_F^2 T_\gamma^5 (C_e - C_x) \Delta f.
 \end{aligned} \tag{3.4}$$

As we can see from the expression, the quantity $\Delta R_{\nu, \text{tot}}$ is larger than zero when $\Delta f = f_{\nu_e} - f_{\nu_x} > 0$ which holds if the reheating temperature is sufficiently low for neutrinos to be fully thermalized and

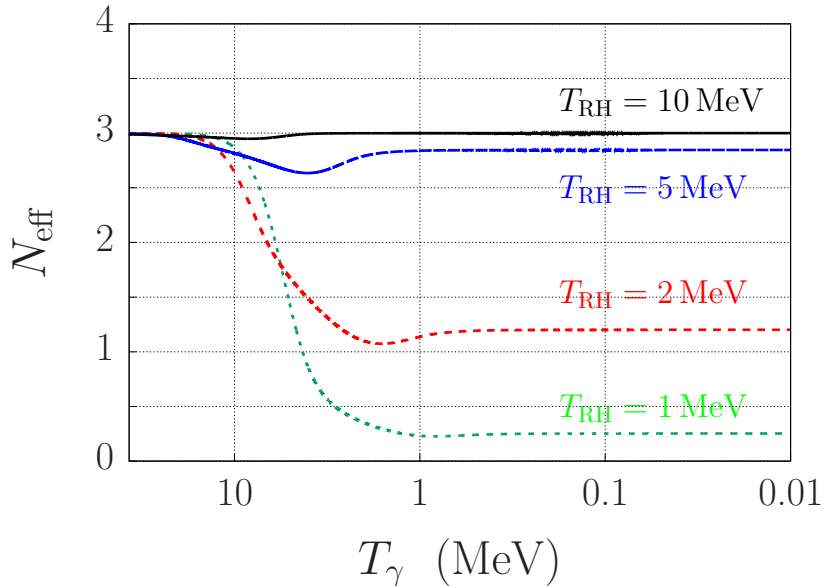


Fig. 2. Time evolution of N_{eff} for each value of T_{RH} . The black solid line is for $T_{\text{RH}} = 10$ MeV, the blue long-dashed line is for $T_{\text{RH}} = 5$ MeV, the red middle-dashed line is for $T_{\text{RH}} = 2$ MeV, and the green short-dashed line is for $T_{\text{RH}} = 1$ MeV. Neutrino oscillation with θ_{12} and neutrino self-interaction are considered in the calculation.

thereby $f_{\nu_e} > f_{\nu_x}$. Consequently, we can see that neutrino oscillation increase the total production rate of neutrinos unless all neutrinos are completely thermalized. Neutrino self-interaction plays a role similar to neutrino oscillation. That is, they equilibrate abundances of neutrinos among themselves and enhance the thermalization of neutrinos in the same way as neutrino oscillation.

We can also see from Fig. 1 that the effect of θ_{13} is much smaller than that of θ_{12} or neutrino self-interaction. This is true independent of the neutrino mass ordering. The relative differences of effects among different mixings can be understood as follows. If the vacuum term (\mathcal{H}_{vac}) dominates other matter terms (\mathcal{H}_{mat}) and neutrino oscillation occur adiabatically, the effective transition rate of neutrinos from one flavor to another (*i.e.* $\nu_\alpha \rightarrow \nu_\beta$ where $\alpha \neq \beta$) due to neutrino oscillation can be written as [22]

$$\Gamma_{\text{trans}} = \frac{1}{4} \sin 2\theta \Gamma_{\text{coll}}, \quad (3.5)$$

where Γ_{coll} is the collision rate of neutrinos. Therefore, the value of the mixing angle solely determines how large oscillation happens in this case. As we can see from Eqs. (2.10)–(2.12), the value of $\sin^2 \theta_{12}$ is almost ten times larger than that of $\sin^2 \theta_{13}$. That is the reason that the effect of θ_{12} on the neutrino thermalization is larger than θ_{13} in the case of normal mass ordering. In the case of inverted mass ordering, neutrino oscillation proceeds via MSW resonance, and non-

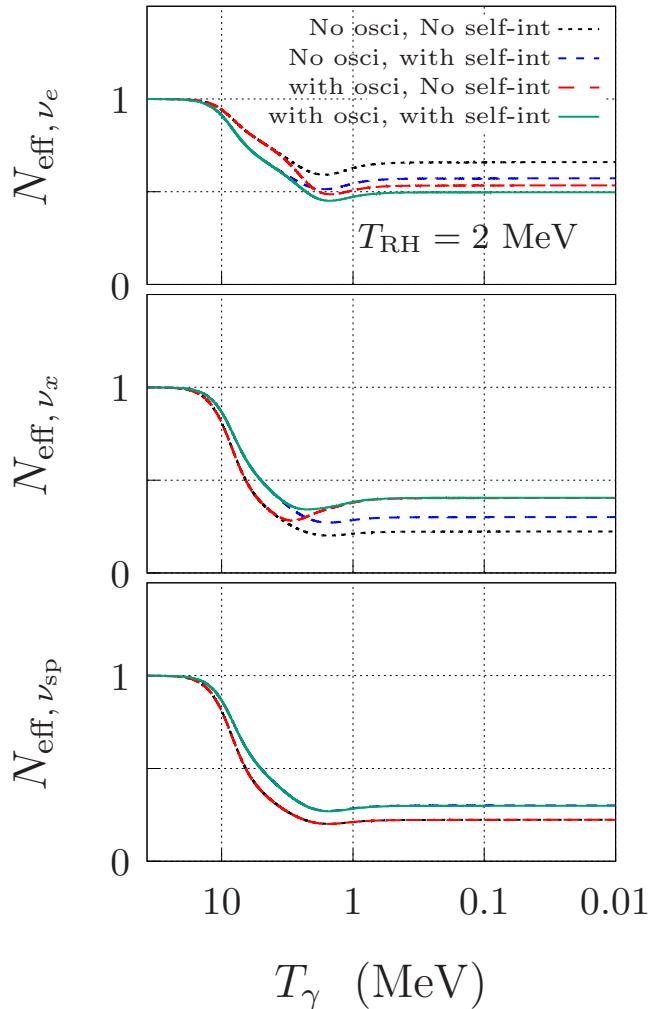


Fig. 3. Time evolution of $N_{\text{eff}, \nu_\alpha}$ for $T_{\text{RH}} = 2$ MeV. N_{eff, ν_e} (top panel) is for ν_e , N_{eff, ν_x} (middle panel) is for ν_x and $N_{\text{eff}, \nu_{\text{sp}}}$ (bottom panel) is for ν_{sp} . In the red long-dashed and green solid lines, neutrino oscillation with θ_{12} is taken into account, and neutrino self-interaction is considered in the blue middle-dashed and green solid lines. In the figure of $N_{\text{eff}, \nu_{\text{sp}}}$, the black short-dashed (blue middle-dashed) and red long-dashed (green solid) lines are overlapping.

adiabatic effects can be important. As for this point, authors in Ref. [9] evaluated the adiabaticity of the MSW resonance and concluded that the non-adiabatic effects are negligible. Therefore, an efficient oscillation should occur when a large population of neutrinos go through the resonance even if we adopt the reactor neutrino mixing θ_{13} . Since the MSW resonance happens at around a temperature of $T_c \sim 5$ MeV for neutrino with $p = \langle p \rangle \sim 3.15 T_\gamma$, we can expect larger oscillation effects in the case of θ_{13} (IO) at $T_{\text{RH}} < T_c$, which in fact can be seen in Fig. 1.

Figure 3 shows the time evolution of N_{eff} , and Fig. 3 is the same as Fig. 2, but for the contribution

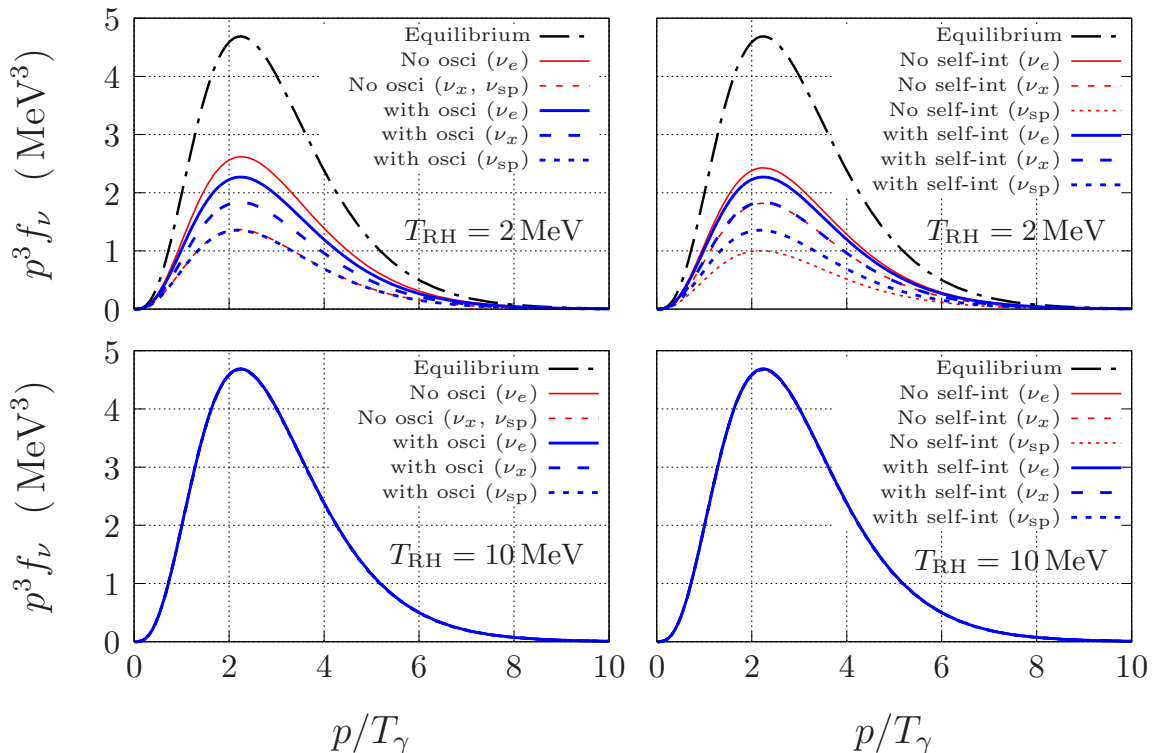


Fig. 4. Final energy spectra of neutrinos. The horizontal axis is the neutrino energy p divided by the photon temperature T_γ . The vertical axis is the differential energy spectrum of neutrinos. In the figure, neutrino self-interaction is considered in the left column, whereas neutrino oscillation with θ_{12} is considered in the right column. We consider θ_{12} in the case with neutrino oscillation in the left column. The thermal spectrum is plotted with the black dot-dashed line. In the top-left panel, the thin red short-dashed and blue thick short-dashed lines are overlapping, while the red thin long-dashed and blue thick long-dashed lines are overlapping in the top-right panel. Also, all plots are almost overlapping in the case of $T_{\text{RH}} = 10$ MeV.

for each neutrino species $N_{\text{eff}, \nu_\alpha}$ ($\alpha = e, x, \text{sp}$). Since the final abundance of neutrinos does not depend on the condition before reheating, we assume that neutrinos have thermal spectra (*i.e.* Fermi-Dirac distributions) at the initial time. We can see from Fig. 2 that the value of N_{eff} decreases until T_{RH} is realized. This is due to the entropy production from decays of the massive particles. The value of N_{eff} then increases at $T_\gamma < T_{\text{RH}}$ until neutrinos are decoupled from other particles at around a few MeV. This corresponds to the upturn behavior in the evolution of N_{eff} . In addition, we can see from the evolution of $N_{\text{eff}, \nu_\alpha}$ in Fig. 3 that neutrino oscillation becomes effective at around a temperature of a few MeV, whereas neutrino self-interaction becomes effective at higher temperature. The former is because, as we have discussed in the previous section, neutrino oscillation with the solar neutrino mixing ($\delta m_{12}^2, \theta_{12}$) are effective when the photon temperature is lower than $T_c \sim 3$ MeV. The latter is due to the reason that the reaction rates of neutrino self-interactions monotonically increase with the photon temperature.

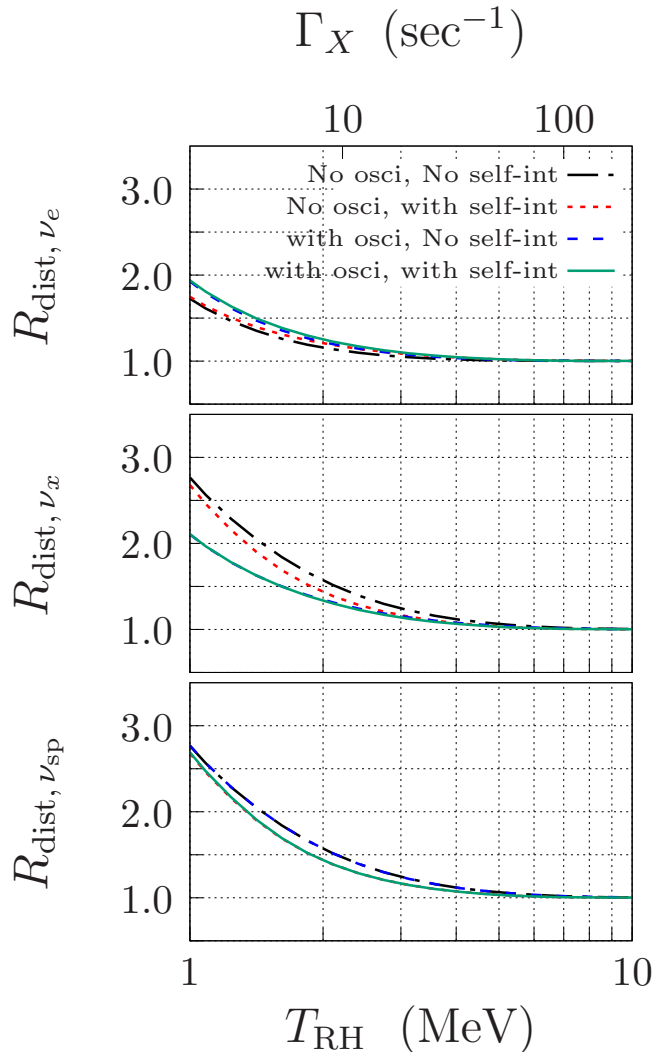


Fig. 5. Dependence of the mean energy of ν_e (top panel), ν_x (middle panel) and ν_{sp} (bottom panel) on T_{RH} . The vertical axis is the distortion parameter R_{dist} for each neutrino species. $R_{\text{dist}} = 1$ corresponds to the thermal spectrum. In the middle panel, the blue long-dashed and green solid lines are overlapping. Also, in the bottom panel, the black dot-dashed (red short-dashed) and blue long-dashed (green solid) lines are overlapping. We consider θ_{12} in the case with neutrino oscillation.

The role of neutrino oscillation and neutrino self-interaction is shown in Fig. 4, where we plot final energy spectra of neutrinos for the cases with and without neutrino oscillation or neutrino self-interaction. The energy spectra are evaluated at $T_\gamma \sim 10^{-2}$ MeV which corresponds to the epoch well after electron annihilation. In the case of $T_{RH} = 2$ MeV, both of these effects decrease the difference in neutrino abundances. On the other hand, if T_{RH} is large enough (*e.g.* $T_{RH} = 10$ MeV), neutrinos are almost completely thermalized well before decoupling. Therefore, neutrino oscillation or neutrino self-interaction plays no role in the final abundance of neutrinos.

Figure 5 shows the dependence of the mean energy of ν_e , ν_x and ν_{sp} (*i.e.* $\rho_{\nu_\alpha}/n_{\nu_\alpha}$) on T_{RH} . The quantity R_{dist} on the vertical axis was introduced to measure the distortion in the final energy spectrum of neutrinos in Ref. [3], and it is defined as

$$R_{\text{dist}} = \frac{1}{3.15 T_{\nu, \text{eff}}} \frac{\rho_\nu}{n_\nu}, \quad (3.6)$$

where $T_{\nu, \text{eff}}$ is the effective temperature of neutrinos $T_{\nu, \text{eff}} = [\frac{4\pi^2}{3\zeta(3)} n_\nu]^{1/3}$. As we can see from this definition, $R_{\text{dist}} = 1$ corresponds to the thermal spectrum, and $R_{\text{dist}} > 1$ indicates a larger mean energy. It can be seen from Fig. 5 that the value of R_{dist} increases as T_{RH} becomes smaller. This is because neutrinos are only produced from the annihilation of electrons $e^- + e^+ \rightarrow \nu_\alpha + \bar{\nu}_\alpha$, and neutrinos in the final state therefore have an energy larger than twice the electron mass. Thus, if neutrinos are mainly produced when the electron mass is not negligible, and the equilibration process $e^\pm + \nu_\alpha \rightarrow e^\pm + \nu_\alpha$ is not effective as in the case of $T_{\text{RH}} \lesssim \mathcal{O}(1)$ MeV, R_{dist} becomes larger than unity. In addition, since ν_e scatter with electrons stronger than ν_x and ν_{sp} due to the charged-current interaction, the energy distribution of ν_e is closer to the thermal spectrum. That is the reason that the relation $R_{\text{dist}, \nu_e} < R_{\text{dist}, \nu_x}$, $R_{\text{dist}, \nu_e} < R_{\text{dist}, \nu_{\text{sp}}}$ holds for a sufficiently small T_{RH} . Furthermore, we can see from Fig. 5 that both neutrino oscillation and neutrino self-interaction increase R_{dist, ν_e} , while decrease R_{dist, ν_x} . This is because neutrino oscillation and neutrino self-interaction equilibrate the neutrino abundances of different flavors as shown in Fig. 4. The reason is as follows: If the final distribution function of neutrinos is changed by a factor of κ (*i.e.* $f_\nu \mapsto \kappa f_\nu$ where $\kappa < 1$ for ν_e and $\kappa > 1$ for ν_x) due to neutrino oscillation or neutrino self-interaction, then the distortion parameter should be also modified by

$$\tilde{R}_{\text{dist}}/R_{\text{dist}} = \frac{\kappa \rho_\nu / \kappa n_\nu}{3.15 (\kappa^{1/3} T_{\nu, \text{eff}})} \left(\frac{\rho_\nu / n_\nu}{3.15 T_{\nu, \text{eff}}} \right)^{-1} = \kappa^{-1/3}, \quad (3.7)$$

where \tilde{R}_{dist} and R_{dist} are distortion parameters for the cases with and without effects of neutrino oscillation or neutrino self-interaction, respectively. Therefore, these effects increase R_{dist, ν_e} and decrease R_{dist, ν_x} as long as neutrino oscillation or neutrino self-interaction is effective. In addition, since the reaction rate of neutrino self-interaction strongly depends on the number density of neutrinos, its effect on R_{dist} becomes small more rapidly than neutrino oscillation as T_{RH} decreases. These effects on R_{dist} can be estimated by comparing neutrino distribution functions in Fig. 4 and is consistent with the results in Fig. 5. On the other hand, since ν_{sp} does not mix with other flavor of neutrinos, they are only affected by neutrino self-interaction.

In the next section, we discuss the light element abundances created in the process of BBN taking our computed neutrino thermalization into account.

IV. BIG BANG NUCLEOSYNTHESIS

As mentioned in Sec. II, incomplete thermalization of neutrinos affects the dynamics of the standard BBN. In this section, we explain the role of neutrinos in the production process of light elements and show our results of BBN obtained by assuming $T_{\text{RH}} \sim \mathcal{O}(1)$ MeV.

A. Formulation of BBN

We have seen in the previous section that the late-time entropy production due to decays of X induces the incomplete thermalization of neutrinos before decoupling. Since neutrinos take part in the weak reaction processes,

$$n \leftrightarrow p + e^- + \bar{\nu}_e, \quad (4.1)$$

$$e^+ + n \leftrightarrow p + \bar{\nu}_e, \quad (4.2)$$

$$\nu_e + n \leftrightarrow p + e^-, \quad (4.3)$$

which interchange ambient neutrons and protons with each other, non-thermal spectra of neutrinos significantly change the freeze-out value of the neutron-to-proton ratio $(n/p)_f \equiv (n_n/n_p)_{T=T_f}$ where n_n and n_p are the number density of neutrons and protons, respectively, whereas T_f is the freeze-out temperature of the processes (4.1)–(4.3). As described later in this section, the theoretical values of light element abundances are very sensitive to the neutron-to-proton ratio before BBN. Therefore, theoretical predictions of the standard BBN should be modified in the Universe with small T_{RH} . Since the predictions of standard BBN is well consistent with the observational values, we can constrain T_{RH} by requiring that the late-time entropy production does not spoil the current success of the standard BBN.

In the case where the massive particles have a hadronic branching ratio, there are additional neutron-proton interchanging processes other than (4.1)–(4.3) via strong interactions caused by injected hadrons $N + H \leftrightarrow N' + H'$ where N and N' are nucleons, and H and H' are mesons or baryons. If the hadronic branching ratio is large enough, the hadronic processes dominantly affect the neutron-to-proton ratio, which result in different light element abundances compared to the case of the 100% radiative decays of the massive particles [3, 23]. In the current study, we consider the hadronic processes involving pions (π^\pm) and nucleons (n, \bar{n}, p, \bar{p}) which are injected from hadronic decays of the massive particles. The energetic hadrons produced in the decay of the massive particles are instantaneously stopped by Coulomb scattering with background electrons/positrons or inverse-Compton like scattering with background photons [23–25]. Therefore,

the hadrons affecting neutron-proton inter-conversions are thermalized, and we can use thermal cross sections for the calculation. As for the hadronic cross sections, we adopt those given in Table.1 of Ref. [23] for the mean values and assume 30% experimental error in each cross section for a conservative treatment (see also Refs. [3, 26]).

In order to follow the evolution of light element abundances, we solve the Boltzmann equations of light elements using the Kawano code [27]. Since some of the nuclear reaction rates in the code are already outdated, we replace them with the latest ones (see Ref. [28] for more information). In addition, we rewrite some equations in the code to allow for the late-time entropy production accompanied by the decays of X . Moreover, since the free neutron decay (*i.e.* the forward process of (4.1)) continues even after the other weak processes of (4.1)–(4.3) decoupled at $T_\gamma \sim T_f$, the value of the neutron-to-proton ratio just before BBN depends on the lifetime of neutrons (see *e.g.* [29]). In the current study, we use the value of the neutron lifetime τ_n reported in Ref. [1]:

$$\tau_n = 880.2 \pm 1.0 \text{ sec} \quad (68\% \text{ C.L.}) \quad . \quad (4.4)$$

As for the observational values of light elements, we adopt the primordial mass fraction of helium ${}^4\text{He}$, Y_p , reported in Ref. [30]:

$$Y_p = 0.2449 \pm 0.0040 \quad (68\% \text{ C.L.}), \quad (4.5)$$

whereas for the observational value of primordial abundance of deuterium D, we adopt the latest value reported in Ref. [31]:

$$\text{D/H} = (2.545 \pm 0.025) \times 10^{-5} \quad (68\% \text{ C.L.}). \quad (4.6)$$

B. Results of BBN: Radiative decay

First we show the results of radiative decay, *i.e.* the hadronic branching ratio $\text{Br} = 0$. In this case, photons and charged leptons emitted from the decay of X are instantaneously thermalized via electromagnetic force, and results of neutrino thermalization and BBN are independent of the mass of X , m_X . In Figs. 6 and 7, the relation between T_{RH} and D/H and Y_p are shown, respectively. We assume the 100% radiative decays of the massive particles in these figures. The baryon-to-photon ratio η_B is the only free parameter in the standard BBN. In the low-reheating-temperature Universe, a baryon number is diluted by the entropy production due to the decays of the massive particles, and hence η_B is decreased by many orders of magnitude. Therefore, we set

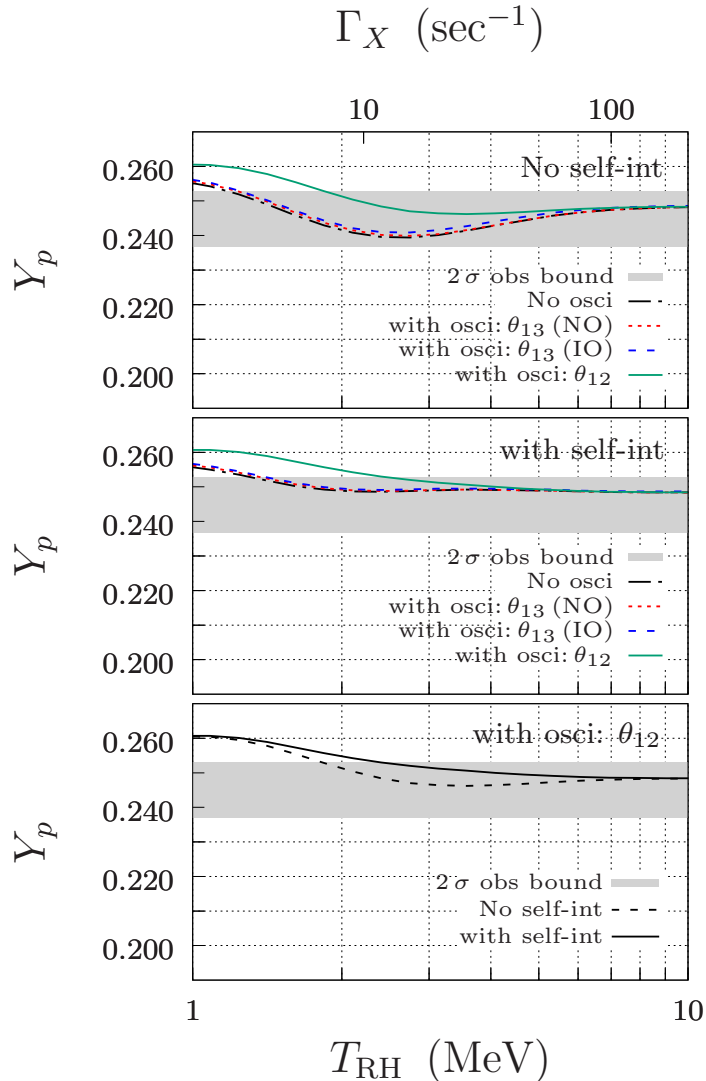


Fig. 6. Relations between T_{RH} and Y_p in the case of the 100% radiative decays of X . We adopt $\eta_B = 6.13 \times 10^{-10}$ in the figure. The top- and middle panels show the effect of neutrino oscillation for the cases without and with neutrino self-interaction, respectively. The black dot-dashed line is for the case without neutrino oscillation, the red short-dashed line is for the case with θ_{13} (NO), the blue long-dashed line is for the case with θ_{13} (IO), and the green solid line is for the case with θ_{12} . The bottom panel shows the effect of neutrino self-interaction when we consider neutrino oscillation with θ_{12} . The black dashed- and solid lines are for the cases without and with neutrino self-interaction, respectively. The gray-shaded region corresponds to the 2σ observational bound.

the large initial value of η_B so that the final value of η_B is consistent with observations of light elements. To plot Figs. 6 and 7, we fix the final value of η_B to the median value reported by Planck collaboration [32]:

$$\eta_B = 6.13 \times 10^{-10}. \quad (4.7)$$

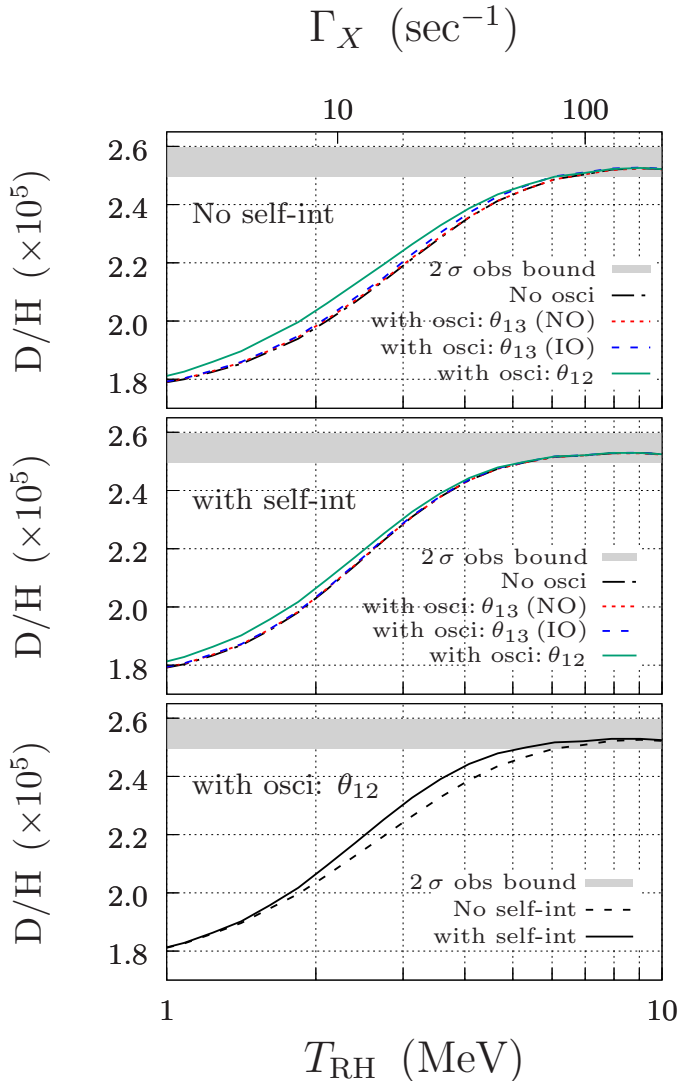


Fig. 7. Same as Fig. 6, but for D/H.

Since almost all neutrons are processed into ${}^4\text{He}$ which is the most stable among light elements, the primordial mass fraction of ${}^4\text{He}$ can be written as $Y_p \equiv \rho_{{}^4\text{He}}/\rho_B \sim 2/\{1 + (n/p)_{\text{BBN}}^{-1}\} \sim 0.25$, where $(n/p)_{\text{BBN}} \equiv (n/p)_f e^{-t/\tau_n}$ is the neutron-to-proton ratio just before deuterium bottleneck opens (*i.e.* $T_\gamma \sim 0.08$ MeV and $t \sim 200$ sec), and the last approximation holds in the standard big-bang cosmology where $(n/p)_{\text{BBN}} \sim 1/7$ [29]. Therefore, the value of $(n/p)_{\text{BBN}}$ almost entirely determines the final abundance of ${}^4\text{He}$. As for the final abundance of D, the value of N_{eff} is also important because it is related to the Hubble parameter (see Eqs. (2.32), (2.34) and (3.1)) and determines when each light element departs from the nuclear statistical equilibrium [33, 34].⁸ In

⁸ We can intuitively understand the dependence of the D abundance on the expansion rate of the Universe in the BBN epoch by focusing on the binding energy of D and ${}^4\text{He}$, *i.e.* $B_{\text{D}} \sim 2.22$ MeV and $B_{{}^4\text{He}} \sim 28.3$ MeV, and the freeze-out temperature of the destroying reactions of D. Since the binding energy of ${}^4\text{He}$ is much larger than that of D, D should burn into ${}^4\text{He}$ (via mass-3 elements, T and ${}^3\text{He}$) as long as the destroying reactions of D such

addition, as we can see from Figs. 6 and 7, the influences of neutrino oscillation and self-interaction on light element abundances are similar, and both of these effects increase Y_p and D/H . In order to understand the numerical results on light element abundances, next we focus on the dynamics of the freeze-out of the neutron-to-proton ratio.

Since nucleons are always non-relativistic, $(n/p)_f$ can be expressed with the freeze-out temperature if T_{RH} is MeV scale as $(n/p)_f \sim \exp(-Q/T_f)$ where $Q \equiv m_n - m_p \sim 1.3$ MeV is the mass difference of nucleons. We note that T_f is determined by the relative values of the neutron-proton inter-converting weak reaction rates Γ_{np} and the Hubble parameter H and is roughly given by $\Gamma_{np}(T_f)/H(T_f) \sim 1$. In the low-reheating-temperature Universe, the total energy density is smaller than that in the standard big-bang cosmology under the same photon temperature due to the incomplete thermalization of neutrinos.⁹ Therefore, the expansion rate of the Universe is also small in the scenario, and this effect delays the decoupling of the processes (4.1)–(4.3) and thereby decreases $(n/p)_f$.

The influence is not only in the Hubble parameter H but also in the reaction rates Γ_{np} . Specifically, the reaction rate of the processes (4.1)–(4.3) can be written as [3]

$$\begin{aligned}\Gamma_{n \rightarrow pe^{-}\bar{\nu}_e} &= K \int_0^{Q-m_e} dp' \left[\sqrt{(p'-Q)^2 - m_e^2} (Q-p') \frac{p'^2}{1 + e^{(p'-Q)/T_\gamma}} (1 - f_{\nu_e}(p')) \right], \\ \Gamma_{ne^+ \rightarrow p\bar{\nu}_e} &= K \int_{Q+m_e}^{\infty} dp' \left[\sqrt{(p'-Q)^2 - m_e^2} (p'-Q) \frac{p'^2}{e^{(p'-Q)/T_\gamma} + 1} (1 - f_{\nu_e}(p')) \right], \\ \Gamma_{n\nu_e \rightarrow pe^-} &= K \int_0^{\infty} dp' \left[\sqrt{(p'+Q)^2 - m_e^2} (p'+Q) \frac{p'^2}{1 + e^{-(p'+Q)/T_\gamma}} f_{\nu_e}(p') \right], \\ \Gamma_{pe^-\bar{\nu}_e \rightarrow n} &= K \int_0^{Q-m_e} dp' \left[\sqrt{(p'-Q)^2 - m_e^2} (Q-p') \frac{p'^2}{e^{-(p'-Q)/T_\gamma} + 1} f_{\nu_e}(p') \right], \\ \Gamma_{pe^- \rightarrow n\nu_e} &= K \int_0^{\infty} dp' \left[\sqrt{(p'+Q)^2 - m_e^2} (Q+p') \frac{p'^2}{e^{(p'+Q)/T_\gamma} + 1} (1 - f_{\nu_e}(p')) \right], \\ \Gamma_{p\bar{\nu}_e \rightarrow ne^+} &= K \int_{Q+m_e}^{\infty} dp' \left[\sqrt{(p'-Q)^2 - m_e^2} (Q-p') \frac{p'^2}{1 + e^{-(p'-Q)/T_\gamma}} f_{\nu_e}(p') \right],\end{aligned}$$

where m_e is the electron mass, and $K \sim (1.636\tau_n)^{-1}$ is a normalization factor whose value is determined by the neutron lifetime τ_n . Of these reaction rates, some depend on f_{ν_e} and others

as DD and DT fusions are effective. For this reason, a small value of N_{eff} (or equivalently a small expansion rate H), attained in the low reheating temperature cases, delays a decoupling of the destroying reactions, and hence a smaller abundance of D remains unburnt. That is the reason that a large expansion rate in the BBN epoch leads to a large abundance of D and vice versa.

⁹ We recall the reader that T_γ determines when light element abundances are to be created since the reaction process $p+n \rightarrow D+\gamma$ responsible for the deuterium production is the first step of BBN, and its backward reaction rate depends on T_γ . For this reason, the values of Γ_{np} and H should not be characterized by the cosmic time but rather by T_γ . That is the reason that a larger value of $N_{\text{eff}} \propto \rho_\nu/\rho_\gamma$ leads to a larger expansion rate of the Universe at the epoch of BBN.

on $1 - f_{\nu_e}$. In the low-reheating-temperature Universe, the neutrino abundance of each flavor is smaller than the case of the standard big-bang cosmology. Therefore, by denoting the reduction of f_{ν_e} due to the incomplete thermalization of neutrinos by Δf_{ν_e} , the following relation holds for sufficiently small $T_{\text{RH}} (< T_{\text{dec}} \sim \mathcal{O}(1) \text{ MeV})$:

$$\left| \frac{\Delta f_{\nu_e}}{(1 - f_{\nu_e})} \right| \ll \left| \frac{\Delta f_{\nu_e}}{f_{\nu_e}} \right| \quad \text{for } f_{\nu_e} \ll 0.5. \quad (4.8)$$

As a result, with such a small value of T_{RH} , the total reaction rate $\Gamma_{np} \equiv \Gamma_{n \rightarrow pe^- \bar{\nu}_e} + \Gamma_{ne^+ \rightarrow p \bar{\nu}_e} + \Gamma_{n\nu_e \rightarrow pe^-} + \Gamma_{pe^- \bar{\nu}_e} + \Gamma_{pe^- \rightarrow n\nu_e} + \Gamma_{p\bar{\nu}_e \rightarrow ne^+}$ becomes smaller than that of the standard big-bang cosmology as written in Ref. [3]. Therefore, this effect accelerates the decoupling of the processes (4.1)–(4.3) and thereby increases $(n/p)_f$. Consequently, the relative magnitude of these two opposite contributions determine the net effect of incomplete thermalization of neutrinos on $(n/p)_f$.

As described in the previous section, neutrino oscillation and self-interaction slightly enhance the neutrino thermalization and increase the total energy density of neutrinos and hence N_{eff} . As a result, the Hubble expansion rate increases due to these effects. In addition, since the ν_e abundance is decreased by the conversion $\nu_e \rightarrow \nu_x$, and only ν_e take part in the reaction processes (4.1)–(4.3), Γ_{np} decreases by considering these effect. Therefore, neutrino oscillation and self-interaction always play a role in delaying the freeze-out of neutron-to-proton ratio and increasing T_f and $(n/p)_f$, which leads to larger values of Y_p and D/H .

As is the case for N_{eff} (see Fig. 1), we can also see from Figs. 6 and 7 that the impact of the solar neutrino mixing $(\delta m_{12}^2, \theta_{12})$ is much larger than that of the reactor neutrino mixing $(\delta m_{13}^2, \theta_{13})$ independent of the neutrino mass ordering. Therefore, the effective two-flavor mixing with $(\delta m_{12}^2, \theta_{12})$ gives a good approximation to the full three-flavor neutrino mixings. For this reason, we hereafter only consider $(\delta m_{12}^2, \theta_{12})$ in the case with neutrino oscillation.

To obtain the observational constraint on T_{RH} , we perform a Monte-Carlo calculation of BBN and χ^2 analysis at each point on the grids of η_B and T_{RH} assuming observational values for Y_p (Ref. [30]) and D/H (Ref. [31]).¹⁰ In the Monte-Carlo calculation, we assume that the reaction rates in the standard BBN, the hadronic reaction rates and the neutron lifetime follow Gaussian distribution and propagate their reported errors to obtain theoretical uncertainties on the light element abundances. Since an allowed region is defined by a parameter space where theoretical

¹⁰ As written in *e.g.* [6, 35], it is technically incorrect to adopt the CMB bound $\eta_B = (6.13 \pm 0.04) \times 10^{-10}$ reported by the Planck collaboration [32] as a prior of BBN because the recombination process depends on the values of N_{eff} and Y_p , and there are correlations between η_B and these quantities. In other words, CMB is not independent from the neutrino thermalization and BBN. In Ref. [32], they adopt the canonical value $N_{\text{eff}} = 3.046$ [18] and Y_p calculated by assuming the standard BBN, which are not necessarily realized in the low-reheating-temperature Universe.

abundances of light elements explain each observational value, we give the lower bound on T_{RH} combining χ^2 values of both D/H and Y_p :¹¹

$$\chi_{\text{D/H}+Y_p}^2 \equiv \chi_{\text{D/H}}^2 + \chi_{Y_p}^2 = \frac{\{(\text{D/H})_{\text{th}}(\eta_B, T_{\text{RH}}) - (\text{D/H})_{\text{obs}}\}^2}{\sigma_{\text{D,th}}^2(\eta_B, T_{\text{RH}}) + \sigma_{\text{D,obs}}^2} + \frac{\{Y_{p,\text{th}}(\eta_B, T_{\text{RH}}) - Y_{p,\text{obs}}\}^2}{\sigma_{Y_p,\text{th}}^2(\eta_B, T_{\text{RH}}) + \sigma_{Y_p,\text{obs}}^2}, \quad (4.9)$$

where $\chi_{\text{D/H}}^2$ and $\chi_{Y_p}^2$ are χ^2 values of D/H and Y_p , respectively. Also, $\sigma_{i,\text{th}}$ and $\sigma_{i,\text{obs}}$ where $i = \text{D/H}$ and Y_p are respectively the theoretical and observational 1σ variance of each light element abundance.

Figure 8 shows the allowed region in the plane of η_B and T_{RH} in the case of the 100% radiative decays. In the current study, we assume that $\chi_{\text{D/H}}^2$ and $\chi_{Y_p}^2$ follow Gaussian distribution. In this case, we can find the lower bound at 95% C.L. on T_{RH} by requiring $\chi_{\text{D/H}+Y_p}^2(\eta_B, T_{\text{RH}}) < 5.991$:

$$T_{\text{RH}} \gtrsim 1.8 \text{ MeV}, \quad (4.10)$$

in the case with both neutrino oscillation and self-interaction. Also, we depict in Fig. 9 the comparison between cases with and without neutrino oscillation or neutrino self-interaction. As can be seen from Fig. 9, we find $T_{\text{RH}} \gtrsim 1.5 \text{ MeV}$ in the case with neutrino oscillation and without self-interaction, whereas $T_{\text{RH}} \gtrsim 0.6 \text{ MeV}$ in the case without neutrino oscillation and with neutrino self-interaction. The BBN bound in the case with neutrino oscillation or self-interaction is tighter than that in the case without them. This is because, as we can see from Fig. 7, neutrino oscillation and self-interaction increase the value of Y_p , and the discrepancy between theoretical and observational values becomes large compared to the case without these effects.

C. Results of BBN: Hadronic decay

As described above, if the massive particles have a branching ratio into hadrons, the constraint on T_{RH} imposed by BBN can be modified compared to when the decays of X are fully radiative (*i.e.* $\text{Br} = 0$). The effects of hadronic decays on light element abundances are shown in Fig. 10 where we plot the dependence of D and ${}^4\text{He}$ abundances on T_{RH} for each value of m_X and Br . The case of $\text{Br} = 0$ in the figure corresponds to the 100% radiative decays of X , which is plotted for reference. In the figure, we assume that the massive particles have a non-negligible branching ratio into $u\bar{u}$ quark pairs to calculate the number of hadrons produced in the decays of X with Pythia 8.2 code.¹²

¹¹ There remains a long-standing problem in the standard BBN that the theoretical prediction of the ${}^7\text{Li}$ abundance is approximately three times larger than that of the observational value if we input the value of the baryon-to-photon ratio from CMB into the calculation of BBN (see *e.g.* [1]). Therefore, we refrain from using the ${}^7\text{Li}$ abundance to constrain T_{RH} in the current study.

¹² We have checked that the BBN bound does not depend on the quark flavor emitted from the massive particles if the mass of the massive particles is much larger than the total mass of emitted quarks (*i.e.* $m_X \gg m_{q_\alpha}$ where m_{q_α} is the quark mass of particular flavor α).

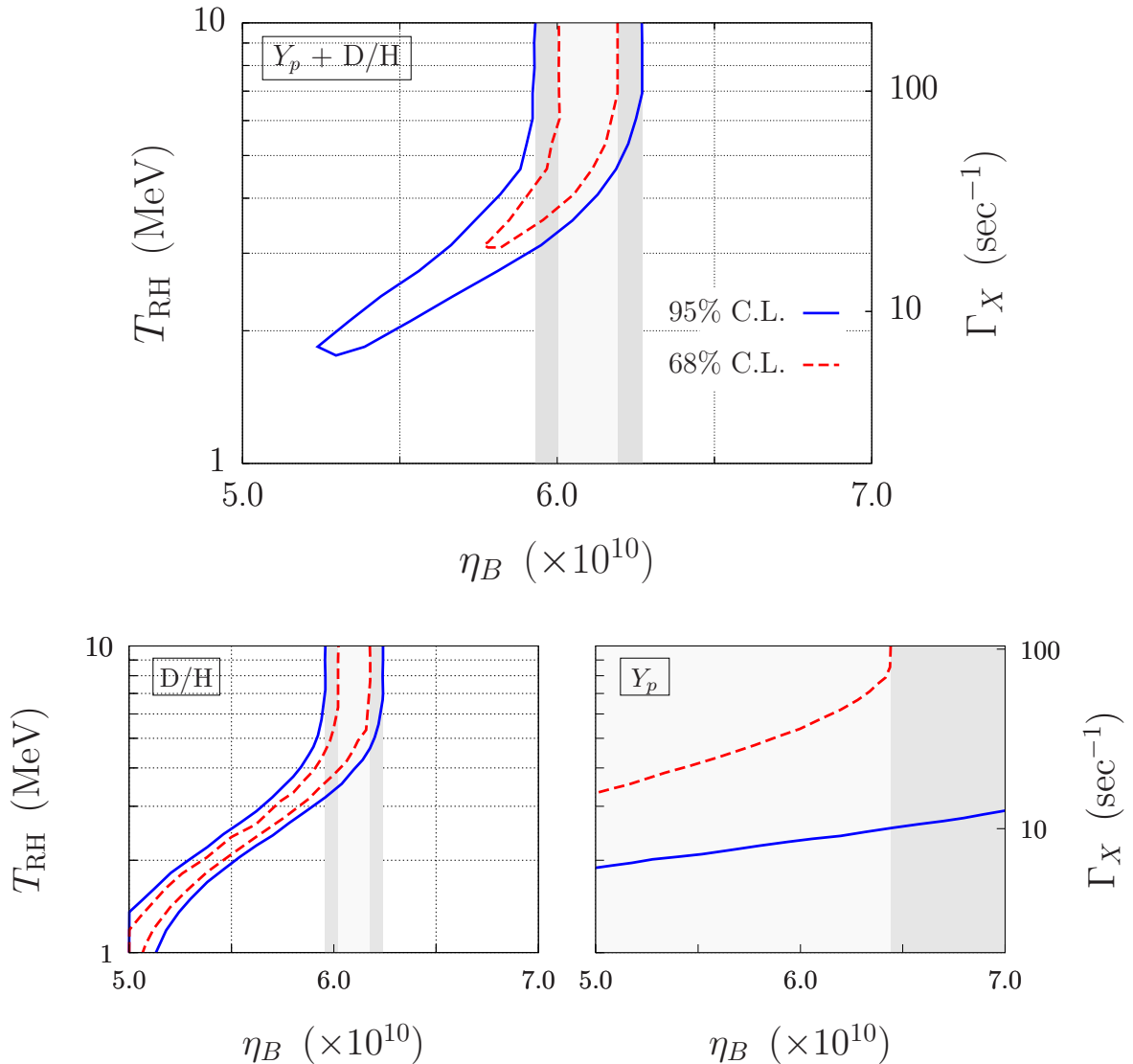


Fig. 8. Allowed region in the (η_B, T_{RH}) plane in the case of the 100% radiative decays of X . The 95% (68%) C.L. contour is plotted with the blue solid (red dashed) line. The outside of the small region surrounded by the blue solid (red dashed) line is excluded at 95% (68%) C.L. The constraint on η_B at 95% C.L. (68% C.L.) in the case of the standard BBN is also shown as the dark (light) shaded region. The top panel shows the allowed region in terms of both Y_p and D/H , whereas the bottom-left and bottom-right panels show those of D/H and of Y_p , respectively. Neutrino oscillation and neutrino self-interaction are considered in the calculation.

Figure 10 shows that both the ${}^4\text{He}$ and D abundances increases due to the hadronic decay effects. The reason is as follows. First, there exist more target protons than target neutrons in the system for $T \lesssim 10$ MeV. This is because the neutron-proton ratio follows $n/p \simeq \exp(-Q/T)$ as long as the neutron-proton exchange reactions through weak interaction keep them in equilibrium,

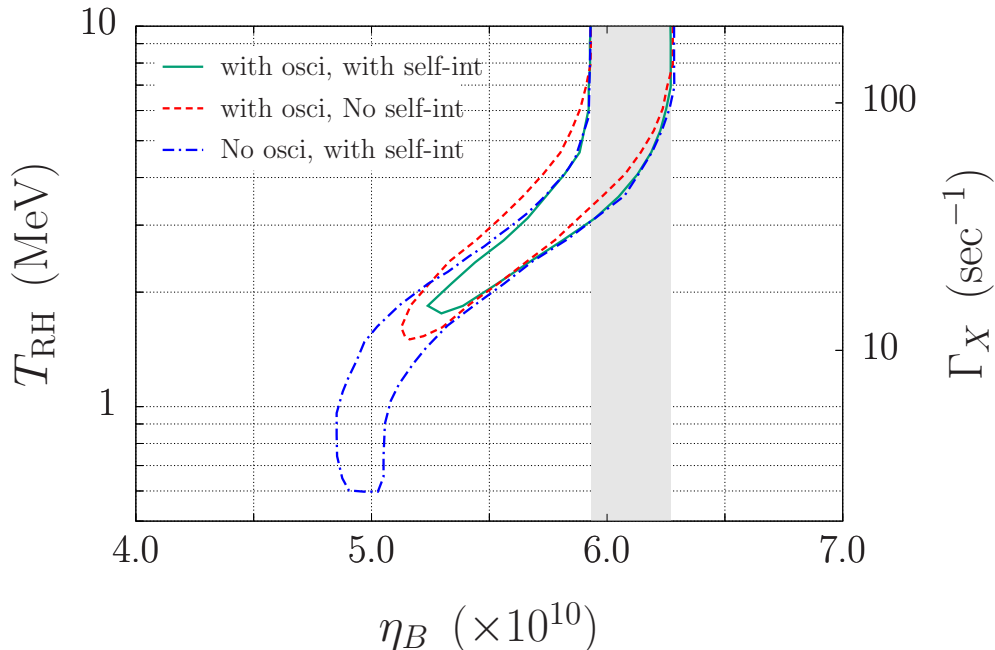


Fig. 9. Comparison of allowed regions in the (η_B, T_{RH}) plane in the cases with or without neutrino oscillation and self-interaction. The outside of the small region surrounded by the contour is excluded at 95% C.L. in each case. The constraint on η_B at 95% C.L. in the case of the standard BBN is also shown as the gray-shaded region. We assume the 100% radiative decays of X . The 95% contour with the green solid line is for the case with both neutrino oscillation and self-interaction, one with the red long-dashed line is for the case only with neutrino oscillation, and one with the short-dashed line is for the case only with neutrino self-interaction.

and n/p is therefore smaller than unity in this epoch. Second, injected hadrons such as pions and kaons extraordinarily exchange ambient protons with neutrons through strong interaction via, *e.g.*

$$\begin{aligned} p + \pi^- &\rightarrow n + \pi^0, \\ n + \pi^+ &\rightarrow p + \pi^0. \end{aligned}$$

We note that the neutral pion π^0 produced in the processes immediately decays into two photons and does not cause the corresponding inverse processes in this epoch. For these reasons, the injected hadrons induce a net flow from p to n . This gives an out of equilibrium abundances of neutron and proton and leads to a larger n/p ratio (see [3, 23] for more detailed discussions). As a result, the ${}^4\text{He}$ and D abundances, which increase with $(n/p)_f$, get larger than those of the standard BBN. In addition, it can be seen from Fig. 10 that the effect of hadronic decays is large for a large Br or a small m_X . Comparing the cases of $m_X = 100$ TeV, Br = 0.001 (red thin dashed) and $m_X = 10$ GeV, Br = 1 (blue thick solid) in Fig. 10, we can see that the discrepancy of D/H or Y_p

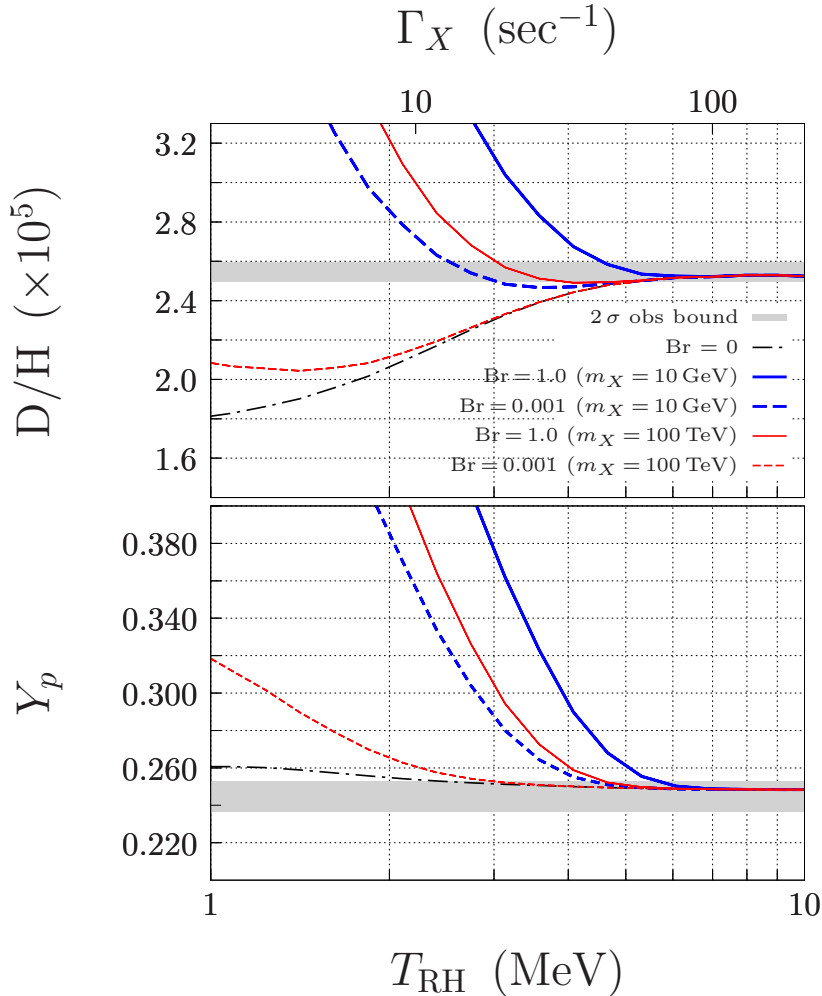


Fig. 10. D/H and Y_p as a function of T_{RH} in the case with hadronic decays of X . The blue thick solid- and dashed lines are for the case of $m_X = 10$ GeV, while the red thin solid- and dashed lines are for the case of $m_X = 100$ TeV. In addition, the blue- and red solid lines are for the case of $\text{Br} = 1$, while the blue- and red dashed lines are for the case of $\text{Br} = 0.001$. For comparison, we also plot the case of $\text{Br} = 0$ with the black dot-dashed line. In the figure, we consider both neutrino oscillation and self-interaction.

between these cases are of the same order or much larger than that of the 2σ observational error if T_{RH} is a few MeV.

To understand the reason, we define the comoving variable for the initial abundance of the massive particles $Y_X = n_X/s$ where n_X is the number density of the massive particles X , and s is the total entropy density of the Universe. If we assume that X dominates the total energy at the initial time and most of it is transferred to radiation components before the reheating is completed,

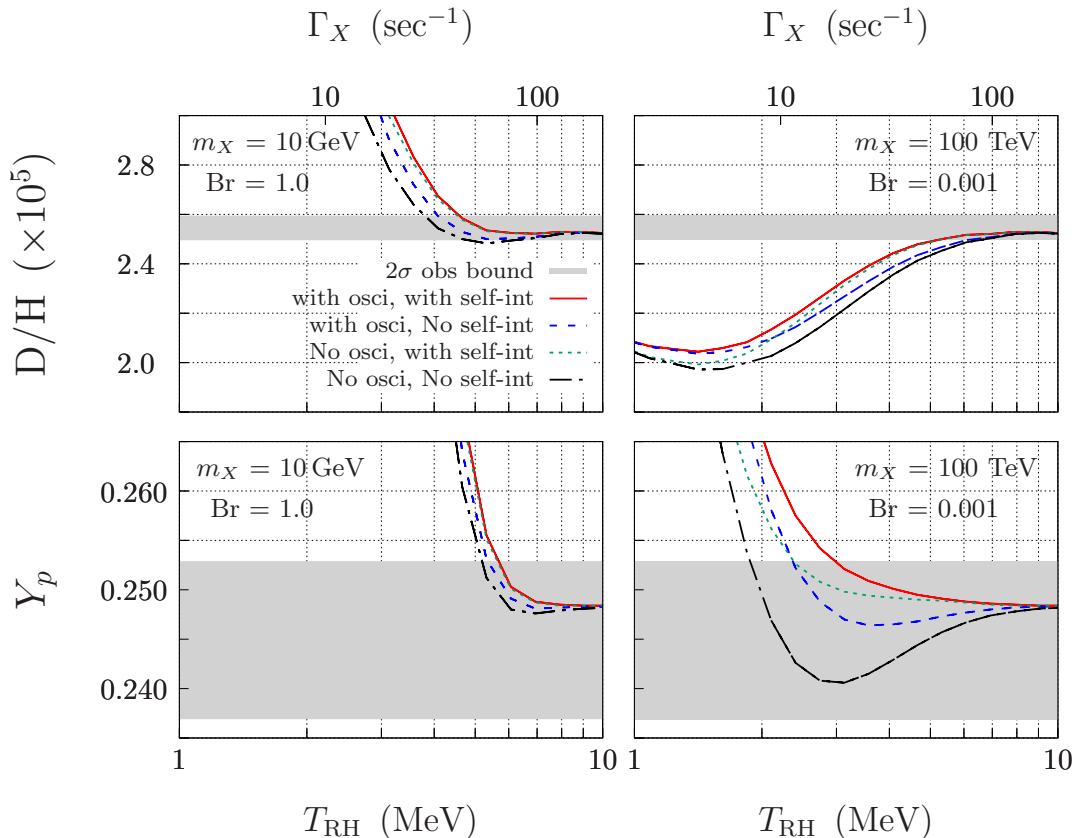


Fig. 11. Effects of neutrino oscillation and self-interaction on D/H and Y_p in the case with hadronic decays of X . We adopt $\eta_B = 6.13 \times 10^{-10}$ in the figure. The red solid- and blue long-dashed lines are for the case with neutrino oscillation, while the green short-dashed and black dot-dashed line are for the case with neutrino self-interaction.

we can write the initial value of Y_X as follows:

$$Y_X = \frac{n_X}{s} \sim \frac{(\frac{\pi^2}{30} g^* T_{\text{RH}}^4)/m_X}{\frac{2\pi^2}{45} g_s^* T_{\text{RH}}^3} \sim \frac{3 T_{\text{RH}}}{4 m_X}, \quad (4.11)$$

where g^* and g_s^* are relativistic degrees of freedom defined by energy and entropy density respectively. In the standard big-bang cosmology, $g^* \sim g_s^*$ holds before electron-positron annihilation sets in. As we can see from the above expression, Y_X gets larger for smaller m_X . In addition, the number of hadrons emitted from the decays of X is almost proportional to $m_X^{0.4}$ (see Ref. [25]), and therefore the total number of hadrons emitted from X is almost proportional to $m_X^{-0.6}$. Since the energetic hadrons instantaneously lose their energy and are thermalized with background particles before inter-converting ambient neutrons and protons, the number of emitted hadrons determine the magnitude of the hadronic-decay effect on BBN. Therefore, the influence of hadronic decays on BBN should be stronger for smaller m_X .

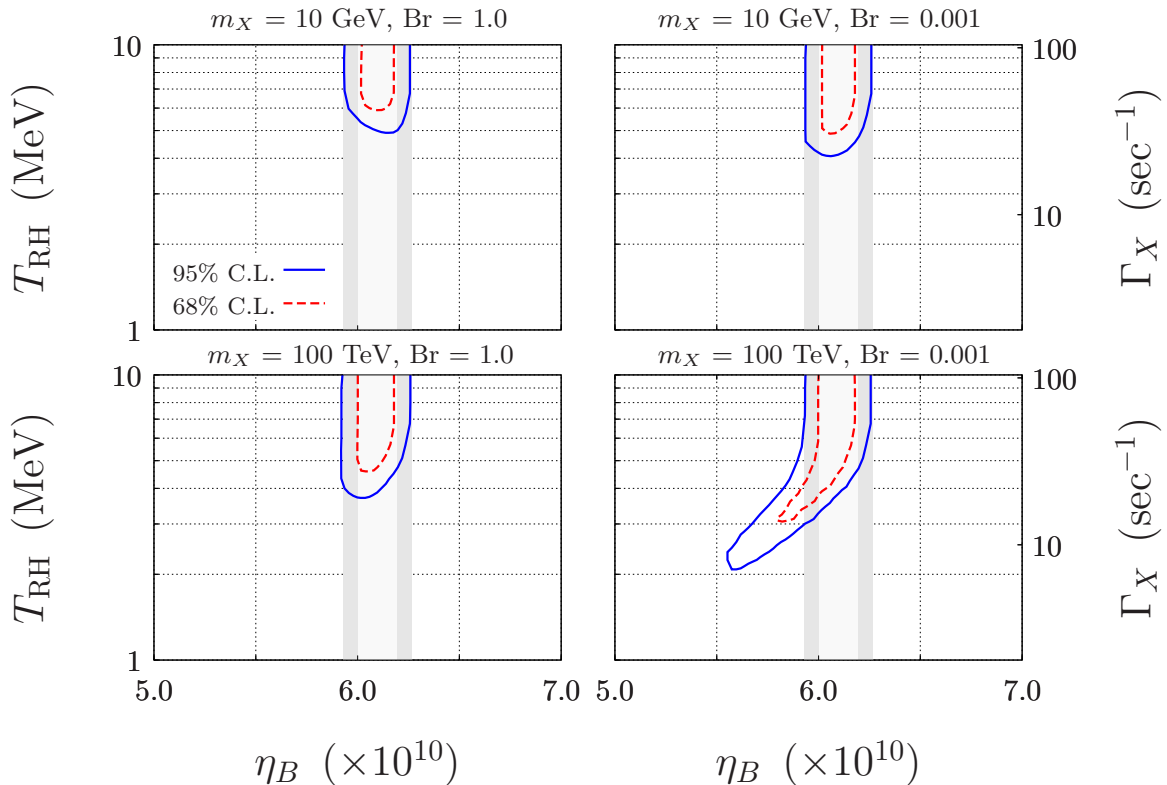


Fig. 12. Same as Fig. 8, but for the case of hadronic decays of the massive particles. The outside of the small region surrounded by the blue solid (red dashed) line is excluded at 95% (68%) C.L. The constraint on η_B at 95% (68%) C.L. in of hadronic decaythe case of the standard BBN is also shown as the dark (light) shaded region.

For the purpose of showing the effects of neutrino oscillation and self-interaction on the light element abundances in the case of hadronic decays, we plot in Fig. 11 the dependence of Y_p and D/H on T_{RH} for $(m_X, Br) = (10 \text{ GeV}, 1.0)$ and $(100 \text{ TeV}, 0.001)$ where we expect large and small effects of hadronic decays, respectively. As we can see from Fig. 11, if T_{RH} is a few MeV, neutrino oscillation and self-interaction affect light element abundances at the level of $\mathcal{O}(10)\%$ for D/H and $\mathcal{O}(1)\%$ for Y_p when $m_X = 10 \text{ GeV}$ and $Br = 1.0$, whereas the correction is $\mathcal{O}(10)\%$ for both cases of D and Y_p when $m_X = 100 \text{ TeV}$ and $Br = 0.001$. Since we give the observational bound on T_{RH} by summing up the χ^2 values of D/H and Y_p , the constraint on T_{RH} should be changed by $\mathcal{O}(1)\%$ when $m_X = 10 \text{ GeV}$ and $Br = 1.0$ and by $\mathcal{O}(10)\%$ when $m_X = 100 \text{ TeV}$ and $Br = 0.001$.

We show in Fig. 12 the allowed region in the same plane as Fig. 8, but in the case when hadronic decays are included. In the figure, we show four representative cases of $(m_X, Br) = (10 \text{ GeV}, 1.0)$, $(10 \text{ GeV}, 0.001)$, $(100 \text{ TeV}, 1.0)$ and $(100 \text{ TeV}, 0.001)$.

A possible minimum value of the reheating temperature $T_{RH, \min}$ in terms of BBN is shown in

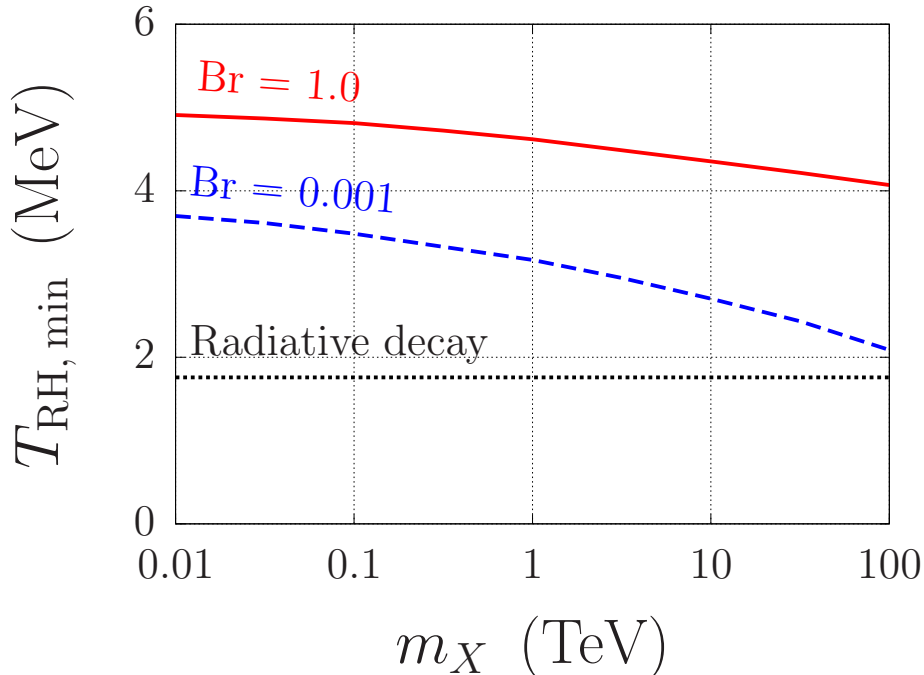


Fig. 13. Lower bound on the reheating temperature $T_{\text{RH}, \text{min}}$ at 95% C.L. as a function of m_X in the case with both neutrino oscillation and neutrino self-interaction. We plot the results in the cases of $\text{Br} = 0.001$ (blue dashed) and 1.0 (red solid). The 100% radiative decay case is also plotted with the black dashed line.

Fig. 13 as a function of m_X . We can see from the figure that the BBN bound is tighter in the case of a small m_X or a large Br . Consequently, we obtain the lower bound on T_{RH} at 95% C.L.:

$$T_{\text{RH}} \gtrsim 4.1 - 4.9 \text{ MeV} \quad \text{for } m_X = 10 \text{ GeV} - 100 \text{ TeV}, \quad (4.12)$$

when the hadronic branching ratio $\text{Br} = 1.0$, whereas

$$T_{\text{RH}} \gtrsim 2.1 - 3.7 \text{ MeV} \quad \text{for } m_X = 10 \text{ GeV} - 100 \text{ TeV}, \quad (4.13)$$

when $\text{Br} = 0.001$ in the case with both neutrino oscillation and neutrino self-interaction. In addition, we find neutrino oscillation and neutrino self-interaction can change the value of $T_{\text{RH}, \text{min}}$ at the level of $\mathcal{O}(1)\%$ for most of the range of m_X in the case of hadronic decays.

V. CONCLUSION

In this paper, we have investigated the possibility that the reheating temperature of the Universe is $\mathcal{O}(1)$ MeV motivated by long-lived massive particles which often appear in the particle physics theory beyond the standard model and induce a late-time entropy production by their decays. In this scenario, neutrinos are not necessarily thermalized well before the beginning of BBN. Hence, the expansion rate of the Universe and weak reaction processes are significantly altered, which changes the freezeout value of the neutron to proton ratio. We have calculated the thermalization process of neutrinos including effects of both neutrino oscillation and neutrino self-interaction (Figs. 1–3), and obtained a lower bound on the reheating temperature $T_{\text{RH}} \gtrsim 1.8$ MeV (95% C.L.) (Fig. 8) in the case of the 100% radiative decay.

On the other hand, if the massive particles also decay into hadrons, there is an additional effect on BBN via inter-conversion of ambient neutron and proton through the scatterings of the hadrons. In this case, the constraint becomes tighter than that of the 100% radiative decay (Fig. 10). Then, we obtained the lower bound $T_{\text{RH}} \gtrsim 2$ MeV–5 MeV (95% C.L.) depending on the masses of the massive particles (10 GeV–100 TeV) and the hadronic branching ratio of the decay (Figs. 12–13).

In addition, we found that neutrino oscillation and neutrino self-interaction increase the efficiency of neutrino thermalization (Figs. 1 and 3) and decrease the exchange rate between neutrons and protons, thereby enhancing the theoretically expected abundances of helium, Y_p (Fig. 6), and deuterium, D/H (Fig. 7). These effects increase the minimum value of the reheating temperature at the level of $\mathcal{O}(10)\%$ in the case of the 100% radiative decays (Fig. 8) and $\mathcal{O}(1)\%$ in most cases of hadronic decay of hadronic decays (Fig. 11).

Finally, let us comment on the future prospects of this study. This time, we only focused on BBN to constrain T_{RH} . On the other hand, as described in Sec. I, CMB and LSS also depend on the expansion rate in the Universe, and therefore have a sensitivity to the neutrino thermalization. In addition, the recombination history depends on the ^4He abundance which is strongly affected by the hadronic decay effects. Therefore, theoretical results of CMB and LSS should be different from those in the case of radiative decay. We will discuss observational constraints on T_{RH} from CMB and LSS in addition to BBN assuming hadronic decays of the massive particles in a forthcoming paper [36].

ACKNOWLEDGMENTS

Numerical computations were carried out on PC clusters at Center for Computational Astrophysics, National Astronomical Observatory of Japan (NAOJ) and Computing Research Center, High Energy Accelerator Research Organization (KEK). KK is supported by JSPS KAKENHI Grants No. JP17H01131, MEXT Grant-in-Aid for Scientific Research on Innovative Areas Nos. JP15H05889, JP18H04594, JP19H05114, and by WPI, MEXT, Japan. The work of RSLH, TT, and SH is supported by the Villum Foundation.

-
- [1] PARTICLE DATA GROUP collaboration, *Review of Particle Physics*, *Phys. Rev.* **D98** (2018) 030001.
- [2] M. Kawasaki, K. Kohri and N. Sugiyama, *Cosmological constraints on late time entropy production*, *Phys. Rev. Lett.* **82** (1999) 4168 [astro-ph/9811437].
- [3] M. Kawasaki, K. Kohri and N. Sugiyama, *MeV scale reheating temperature and thermalization of neutrino background*, *Phys. Rev.* **D62** (2000) 023506 [astro-ph/0002127].
- [4] K. Ichikawa, M. Kawasaki and F. Takahashi, *The Oscillation effects on thermalization of the neutrinos in the Universe with low reheating temperature*, *Phys. Rev.* **D72** (2005) 043522 [astro-ph/0505395].
- [5] P. F. de Salas, M. Lattanzi, G. Mangano, G. Miele, S. Pastor and O. Pisanti, *Bounds on very low reheating scenarios after Planck*, *Phys. Rev.* **D92** (2015) 123534 [1511.00672].
- [6] S. Hannestad, *What is the lowest possible reheating temperature?*, *Phys. Rev.* **D70** (2004) 043506 [astro-ph/0403291].
- [7] K. Ichikawa, M. Kawasaki and F. Takahashi, *Constraint on the Effective Number of Neutrino Species from the WMAP and SDSS LRG Power Spectra*, *JCAP* **0705** (2007) 007 [astro-ph/0611784].
- [8] F. De Bernardis, L. Pagano and A. Melchiorri, *New constraints on the reheating temperature of the universe after WMAP-5*, *Astropart. Phys.* **30** (2008) 192.
- [9] L. Johns, M. Mina, V. Cirigliano, M. W. Paris and G. M. Fuller, *Neutrino flavor transformation in the lepton-asymmetric universe*, *Phys. Rev.* **D94** (2016) 083505 [1608.01336].
- [10] P. F. de Salas, D. V. Forero, C. A. Ternes, M. Tortola and J. W. F. Valle, *Status of neutrino oscillations 2018: 3σ hint for normal mass ordering and improved CP sensitivity*, *Phys. Lett.* **B782** (2018) 633 [1708.01186].
- [11] B. H. J. McKellar and M. J. Thomson, *Oscillating doublet neutrinos in the early universe*, *Phys. Rev.* **D49** (1994) 2710.
- [12] G. Sigl and G. Raffelt, *General kinetic description of relativistic mixed neutrinos*, *Nucl. Phys.* **B406** (1993) 423.
- [13] S. Hannestad, R. S. Hansen, T. Tram and Y. Y. Y. Wong, *Active-sterile neutrino oscillations in the early Universe with full collision terms*, *JCAP* **1508** (2015) 019 [1506.05266].
- [14] L. Wolfenstein, *Effects of Matter on Neutrino Oscillations*, *AIP Conf. Proc.* **52** (1979) 108.
- [15] S. P. Mikheyev and A. Y. Smirnov, *Resonant neutrino oscillations in matter*, *Prog. Part. Nucl. Phys.* **23** (1989) 41.
- [16] S. Hannestad, I. Tamborra and T. Tram, *Thermalisation of light sterile neutrinos in the early universe*, *JCAP* **1207** (2012) 025 [1204.5861].
- [17] S. Hannestad, R. S. Hansen and T. Tram, *Can active-sterile neutrino oscillations lead to chaotic behavior of the cosmological lepton asymmetry?*, *JCAP* **1304** (2013) 032 [1302.7279].
- [18] G. Mangano, G. Miele, S. Pastor, T. Pinto, O. Pisanti and P. D. Serpico, *Relic neutrino decoupling including flavor oscillations*, *Nucl. Phys.* **B729** (2005) 221 [hep-ph/0506164].

- [19] P. F. de Salas and S. Pastor, *Relic neutrino decoupling with flavour oscillations revisited*, *JCAP* **1607** (2016) 051 [1606.06986].
- [20] N. F. Bell, R. R. Volkas and Y. Y. Y. Wong, *Relic neutrino asymmetry evolution from first principles*, *Phys. Rev.* **D59** (1999) 113001 [hep-ph/9809363].
- [21] K. Enqvist, K. Kainulainen and M. J. Thomson, *Stringent cosmological bounds on inert neutrino mixing*, *Nucl. Phys.* **B373** (1992) 498.
- [22] R. Foot and R. R. Volkas, *The Exact parity symmetric model and big bang nucleosynthesis*, *Astropart. Phys.* **7** (1997) 283 [hep-ph/9612245].
- [23] M. H. Reno and D. Seckel, *Primordial Nucleosynthesis: The Effects of Injecting Hadrons*, *Phys. Rev.* **D37** (1988) 3441.
- [24] K. Kohri, *Primordial nucleosynthesis and hadronic decay of a massive particle with a relatively short lifetime*, *Phys. Rev.* **D64** (2001) 043515 [astro-ph/0103411].
- [25] M. Kawasaki, K. Kohri and T. Moroi, *Big-Bang nucleosynthesis and hadronic decay of long-lived massive particles*, *Phys. Rev.* **D71** (2005) 083502 [astro-ph/0408426].
- [26] M. Pospelov and J. Pradler, *Metastable GeV-scale particles as a solution to the cosmological lithium problem*, *Phys. Rev.* **D82** (2010) 103514 [1006.4172].
- [27] L. Kawano, *Let's go: Early universe. 2. Primordial nucleosynthesis: The Computer way*, .
- [28] M. Kawasaki, K. Kohri, T. Moroi and Y. Takaesu, *Revisiting Big-Bang Nucleosynthesis Constraints on Long-Lived Decaying Particles*, *Phys. Rev.* **D97** (2018) 023502 [1709.01211].
- [29] G. Steigman, *Primordial Nucleosynthesis in the Precision Cosmology Era*, *Ann. Rev. Nucl. Part. Sci.* **57** (2007) 463 [0712.1100].
- [30] E. Aver, K. A. Olive and E. D. Skillman, *The effects of He I $\lambda 10830$ on helium abundance determinations*, *JCAP* **1507** (2015) 011 [1503.08146].
- [31] E. O. Zavarygin, J. K. Webb, S. Riemer-Sørensen and V. Dumont, *Primordial deuterium abundance at $z_{abs} = 2:504$ towards Q1009+2956*, *J. Phys. Conf. Ser.* **1038** (2018) 012012 [1801.04704].
- [32] PLANCK collaboration, *Planck 2018 results. VI. Cosmological parameters*, 1807.06209.
- [33] R. Esmailzadeh, G. D. Starkman and S. Dimopoulos, *Primordial nucleosynthesis without a computer*, *Astrophys. J.* **378** (1991) 504.
- [34] M. S. Smith, L. H. Kawano and R. A. Malaney, *Experimental, computational, and observational analysis of primordial nucleosynthesis*, *Astrophys. J. Suppl.* **85** (1993) 219.
- [35] J. Hamann, S. Hannestad, G. G. Raffelt and Y. Y. Y. Wong, *Sterile neutrinos with eV masses in cosmology: How disfavoured exactly?*, *JCAP* **1109** (2011) 034 [1108.4136].
- [36] T. Hasegawa, N. Hiroshima, K. Kohri, S. Wang, R. S. Hansen, T. Tram et al., *In preparation, 2019*, .